Characterization and Separation of Suspension Cells by Isoacoustic Focusing

Rezayati Charan, Mahdi

2023

Document Version:
Publisher's PDF, also known as Version of record

Characterization and Separation of Suspension Cells by Isoacoustic Focusing

Mahdi Rezayati Charan

LUND
UNIVERSITY

DOCTORAL DISSERTATION
by due permission of the Faculty of Engineering, Lund University, Sweden. To be defended in E:1406, Ole Römers väg 3, Lund, November 10th 2023 at 09:00.

Faculty opponent
Professor Martin Viklund

They lived a life under the threat of nothingness as if they lived under no threat

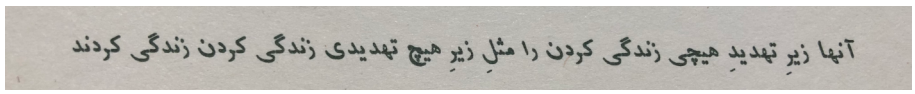

Sadeghieh dar Bayate Esfahan.

Public defence
November 10th 2023, 09:00 in E:1406, Ole Römers väg 3, 223 62 Lund, Sweden.

Advisor
Associate Professor Per Augustsson
Department of Biomedical Engineering, Lund University, Sweden

Co advisors
Assistant Professor Maria Antfolk and Dr. Ola Jakobsson
Department of Biomedical Engineering, Lund University, Sweden

Faculty opponent
Professor Martin Viklund
Department of Applied Physics, KTH Royal Institute of Technology, Sweden

Examination board
Professor Nicole Pamme
Department of Materials and Environmental Chemistry, Stockholm University, Sweden
Senior Lecturer Caroline Adiels
Department of Physics, University of Gothenburg, Sweden
Associate Professor Peter Jönsson
Department of Chemistry, Lund University, Sweden
Deputy member: Professor Jonas Tegenfeldt
Department of Physics, Lund University, Sweden

Chairman
Associate Professor Johan Nilsson
Department of Biomedical Engineering, Lund University, Sweden

Cover illustration
Illustration of isoacoustic focusing. Illustration by Teresa Heintz.

ISBN: 978-91-8039-857-2 (print)
ISBN: 978-91-8039-858-9 (pdf)
Report No. 5/23
ISRN: LUTEDX/TEEM-1137-SE
Printed in October 2023 by Tryckeriet i E-huset, Lund, Sweden

Popular Science

In recent two decades, microfluidic platforms have received much attention for their unique capability to analyze different types of cells in biology and medicine. Microfluidic stands for fluidic channels with micrometer dimensions. To picture it better, note that the diameter of human hair is around 50 micrometers. During this revolutionary time, many studies in different research groups have used various methods based on cell size, deformability, magnetic and optical properties, and other biophysical properties to distinguish cells from each other. The idea is that the isolation of target cells, such as cancer cells, from a complex mixture of cells helps the researcher to study those target cells and improve the disease treatment process. The work of this thesis reveals more details about an enabling method, called isoacoustic focusing, to characterize and separate cancer cells from normal cells based on their acoustic signature. This characteristic, which depends on the cells' density and compressibility, demonstrates how much they would be affected by sound waves in the microchannel and facilitates cell separation in a size-insensitive format. Moreover, with this approach, we can shed light on the alteration of cells' "biophysical fingerprints" in different conditions, which is extremely important in some diseases such as cancer. Another advantage of this method is that it is label-free and doesn't require any chemical labels to capture cancer cells. This method can potentially be developed into a handheld device that counts different blood components. This tiny device can replace the common complete blood count to make it easier and faster to do a test. In that technique, expensive and time-consuming labeling is necessary; however, with this method complete count of red blood cells and different types of white blood cells present in a patient's bloodstream can be done without any labeling.

The isoacoustic focusing device has a microfluidic channel of silicon and glass that vibrates at high frequency. The vibration creates sound waves that carry energy and can generate acoustic forces. As cells flow through the channel, they are pushed to a specific position depending on how they interact with the acoustic forces generated by the vibration. This equilibrium location, called isoacoustic point, is similar to its counterpart in centrifugation. Dur-

ing density gradient centrifugation, cells sediment through layers of liquids of different densities formed by a gradient medium until reaching their neutral buoyancy points called isopycnic points [Figure 1(a)]. In the iso-acoustic focusing channel, the controlling parameter of this cell-specific position, instead of the density, is acoustic impedance. To translate the principle and create a gradient of acoustic impedance in the microchannel, we laminate two liquids of the different acoustic impedances side by side. The liquid with the higher acoustic impedance occupies the center of the channel, and the one with a lower acoustic impedance stays on the sides. In theory, and based on what we know from Newtonian physics, this kind of gradient would eventually collapse because the central liquid, which is denser, would relocate to the bottom of the microchannel simply because of gravity. However, the acoustic forces generated by high-frequency vibrations of the channel prevent that from happening and stabilize two streams against gravity. While two streams pass the channel, the central liquid diffuses to the side and forms a gradient of acoustic impedance where cells move laterally toward their isoacoustic point [Figure 1(b)].

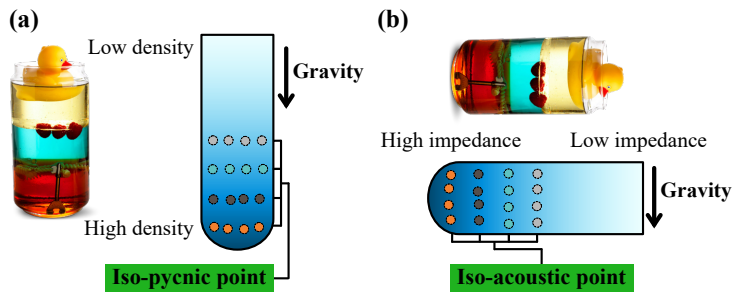

Figure 1: An analogy of density gradient centrifugation and isoacoustic focusing. (a) In density gradient centrifugation, the centrifugal force pushes the cells to locations in the medium of continuous density gradient where they become neutrally buoyant. (b) In iso-acoustic focusing, the interplay of acoustic force and diffusion shapes a smooth gradient of acoustic impedance in the microchannel despite the gravitational force. Individual cells move transverse to the flow toward their isoacoustic point, at which the acoustic contrast between the cell and the surrounding liquid becomes zero, and the sideways displacement ceases.

This technique successfully distinguishes three different types of white blood cells (monocytes, lymphocytes, and neutrophils) even though monocytes and neutrophils are very similar in size. We have used these charted properties to isolate lymphocytes and monocytes directly from undiluted blood. Lymphocytes and monocytes are critical components of the immune system, and separating them from whole blood is often a first step towards performing complex biological analyses and treatments such as cytokine release, genome sequencing, and cell therapies. In addition to analyzing red and white blood cells, with

this technique, we uncover a lower acoustic impedance for different cancer cells than normal cells in the blood, opening doors for improved cancer cell separation. To reach a perfect separation of target cells with this technique, it is crucial to map the acoustically induced motion of cells in different suspension media. The work herein thoroughly investigates the three-dimensional motion of cells for media of altered acoustic impedances in a microchannel. To track cells in three dimensions, we first image them with a camera connected to a microscope while they are moving. Based on how much their shape becomes defocused, we record three-dimensional trajectories. To fully characterize a cell's motion in an acoustic cavity as such, we need access to the cell's biophysical parameters, including size, density, and compressibility. In the last part of this thesis, we integrated a density gradient centrifugation module to measure the density of cells before they enter the isoacoustic focusing channel. The known density of cells while flowing the channel and their isoacoustic point were used to derive the compressibility of cells. Finally, the work of this thesis provides new insight into the characterization and separation of cells by using gradient acoustic impedances. Hopefully, these findings will pave the way for a better understanding of cancer and a new size-insensitive label-free cancer cell separation tool.

Abstract

Enabling techniques for separating target cells, such as subgroups of white blood cells and cancer cells from blood and other body fluids, are necessary for lab work facilitation, inline integration with high-end bioanalytical instrumentation, and for point-of-care or home testing. The work of this thesis addresses this need by further studying an equilibrium-based ultrasonic wave-based technology called isoacoustic focusing to characterize and gain access to cells. In this size-insensitive technique, cells are suspended in a microchannel filled with an inhomogeneous medium where the interaction of diffusion, gravity, and acoustic radiation shapes a smooth gradient profile for the acoustic impedance of the media orthogonal to the flow. While flowing, the acoustic radiation force pushes cells towards their isoacoustic point where the acoustic contrast and radiation force become zero and cells' acoustically induced sideways displacement ceases. The first two included papers in this thesis uncover in detail the acoustophoretic motion of cells suspended in homogeneous and inhomogeneous media in a stop-flow condition. Cell three-dimensional trajectories were measured by a defocused-image tracking approach, and the technique's applicability for tracking cells was assessed by determining the associated error when measuring the out-of-image-plane component of the tracks. In a homogeneous medium, for cells with near-zero acoustic contrast, strong effects of buoyancy and acoustic streaming were observed, and small distributions of cell properties within a population resulted in large differences in the cell motion patterns. The second article shows how cells migrate towards their iso-acoustic point in acoustic impedance gradient media while acoustic streaming is substantially suppressed. This enabled the readout of the effective acoustic impedance of neutrophils and K562 cancer cells. A numerical model was introduced to estimate the acoustic energy density in the acoustic impedance gradient media by tracking particles of known properties. To examine cell separation based on the knowledge acquired in the two first studies, the third paper presents the use of gradient acoustic focusing and dense media containing iodixanol to purify peripheral blood mononuclear cells (PBMCs) from whole blood in a label-free and flow-through format. By modifying the

medium and thus tuning the contrast factor of the cells, PBMCs were enriched relative to RBCs by a factor of 3600 to 11000 and with a separation efficiency of 85%. Such a level of RBC depletion is high compared to most other microfluidic methods and similar to density centrifugation. In the fourth Paper, we show that cell compressibility can be determined at the isoacoustic point by an independent measurement of the density of each cell. Cells were pre-sorted off-chip in linear, continuous, and reproducible density gradients, and fractions with known densities were fed into an isoacoustic focusing device. The relation between density and compressibility for two cell types was investigated, and it was found that for increasing density of K562 cells, the compressibility decreases. For neutrophils, the compressibility was measured, and a slight change was observed with increasing density.

Preface

This dissertation is divided into two parts. The first part serves as an introduction to the relevant concepts within the field and ends with a brief summary of four Papers that are the core of this thesis and future works. The second part consists of the following four Papers:

Paper I **Mahdi Rezayati Charan**, Filip Berg, Per Augustsson, "Acoustofluidic Three-Dimensional Motion of Suspended Cells at Near-Zero Acoustic Contrast in Homogeneous Media," in *Phys. Rev. Applied*, 19, 014046 – Published 18 January 2023.

Paper II **Mahdi Rezayati Charan**, Per Augustsson, "Acoustophoretic Characterization and Separation of Blood Cells in Acoustic Impedance Gradients," in *Phys. Rev. Applied*, 20, 024066 – Published 25 August 2023.

Paper III Julia Alsved[†], **Mahdi Rezayati Charan**[†], Pelle Ohlsson, Anke Urbansky, Per Augustsson, "Label-Free Separation of Peripheral Blood Mononuclear Cells from Whole Blood by Gradient Acoustic Focusing," manuscript submitted for publication. [†]Equal contribution.

Paper IV **Mahdi Rezayati Charan**, Oskar Andersson, Ola Jakobsson, Per Augustsson, "Microfluidic Compressibility Cytometry Using Isoacoustic Focusing Integrated with Density Centrifugation," manuscript.

Author's contribution
In Papers I and II, the author planned and performed the experiments, analyzed the data, and prepared the manuscript. In Paper III, the author shared the contribution of planning and performing experiments, data collection, result analysis, and preparing the manuscript. In Paper IV, the author planned and performed major parts of the experiments, analyzed the data, and prepared the manuscript.

Acknowledgements

First and foremost, I would like to express my heartfelt gratitude to my supervisor, Per Augustsson, for his patience, support, guidance, and mentoring throughout my PhD studies. I am grateful to Per for all that I learned from him. The "all" in the previous sentence includes very basic tools in the lab, among other things, such as working with Transistor-Transistor-Logic (TTL) signals. Per has been so kind to me, and I know that he would not be so happy if I extended this paragraph. Therefore, you need to be able to read between the lines.

In Per's research group, I was lucky to be surrounded by very nice people. I thank Ola, Cecilia, Wei, Enrico, Richard, Franzi, and Oskar for their help whenever it was needed. With them being around, an inclusive and comfortable environment was created in the corridor where our offices were located. I am truly blessed by their support in different forms. I think it becomes a lengthy paragraph to mention a good memory of each of you; therefore, I will do it when I give this book to you. In particular, I thank Richard for always bringing me chewing gum with a watermelon taste from Bavaria and the Persian carpet mouse pad, which "Yeah, man. It really tied the desk together". Richard, you are the best of us, my friend, remember. Now, here comes the difficult part of extending my deep gratitude to my lovely colleague and friend, Enrico. Once I told him about a very strange and striking statement: "Language is fascist", and we often had good conversations about it. The language compels me to write: I wish everyone to have a colleague and friend like "mio caro" Enrico. "Indeedio", I hug him to forget the prison of language.

I would like to thank all my present and past colleagues at the Department of Biomedical Engineering for their good company and help along the way. When I arrived in Sweden, Hamid kindly guided me through different things, and I am very much grateful for his big heart. At BME, I occasionally had interesting conversations with Leif about various topics, including cinema, music, books, and food. They will stay with me. Ulrika was so kind to me that I can't express the amount. I thank Axel for all the milling and printing. The Persian couple (Azin & Hesam) whose smile was adorable, I thank them very much for their

humble smiles. It is a two-way street, Johan; thank you for being an absolutely excellent office mate. Nebojsa (a.k.a. Zlatna Dzigercia) was the first person I met at BME when I mistakenly ended up in his office in the search for Per. I thank him for his friendship, fika breaks, and all the laughter. Once, I wrote in my diaries that a good thing about tall people is when you hug them, you place your head on their hearts. One day we will do a cruise tour of the Caspian Sea while eating caviar when the mission is done. Now I remember it is not fair that I have not mentioned Megan, Maria, Franziska, Anke, Flix, Pelle, Jonathan, Andreas, Johans, Thomas, Ammy, Désirée, Julia, Thierry, Amal, Michael, Jia... forgive me if I may have forgotten you.

Upstairs at EIT, I have some friends too. There are some rumors that say every Persian in Lund knows me, but "they can not be serious". It is not true; believe me. I am laughing while typing. Anyway, I thank Mr. and Mrs. B, MJ, Iman, Arturo, Laura, and Juan for sharing their time with me on different occasions. Mr. and Mrs. B, you dwell in my heart. On Fridays after lunch with Juan, we had a short coffee break to analyze different things, such as our tennis performance. Yo, bro, you are not going to win if you play once a week. "Qué mirás? Andá para allá."

Lund, with all its hazelnut trees, introduced me to some other close friends. I thank them for their generosity, hospitality, and patience. "Boosobaghal" to Ken (f.k.a. Milad), Niloofar, MirSeyedNazari, and the man of "Anargerdoo" Mr. GorandanSaraei. Sara, when you read this, please promise you will take me to Nepal for the mountains. Lund also brought Teresa into my life for the last nine months; being with her was full of inspiring lessons. I heartily appreciate her eye-opening company. "Wo, wo leuchten sie denn, die fernhintreffenden Sprüche?" Before I jump to the last paragraph, I would like to send my warm greetings to my amazing friends in the Netherlands, Ali J., Ali H., Nina, and Saba, with whom I had very unique times.

To my parents, Razieh and Habib, I only can write in my mother tongue Taleshi: "Jani Ghoorban, Chami ra Bamardim". Hadi, the essence of the Charan brothers, belongs to "beyondness" and I can not explain that. This thesis is dedicated to those who are portrayed on page III. Similar to Sadeghieh dar Bayate Esfahan that page does not have a number.

Mahdi.

Contents

Part I

Overview of Research Field

Chapter 1

Introduction

I started my Ph.D. project with a whiteboard sketch of the entire experimental setup and an email: "I want you to become a world-leading expert on the density and compressibility of cells and their different parts! A smile emoji." Although I never asked about "their different parts", it took me almost five years, through thick and then, to get my feet wet measuring the density and compressibility of suspension cells in the last Paper included in this thesis. To be precise, I must mention that halfway through my Ph.D. project, We collaborated with a group at ETH Zürich to use my setup for separating yeast cells based on their densities. In that project, density was manipulated for temperature-sensitive mutants and measured by capillary centrifugation. After all, I think serving the goal of that email needs more time, hard work, and patience; however, I learned that our acoustofluidics community lacks a systematic chart for the density and compressibility of cells. Besides cell size, these two parameters are the backbone of active cell manipulation in the field, enabling us to predict cells' motion in different settings. The idea behind my Ph.D. project was to characterize suspension cells in a technique called isoacoustic focusing to bring more attention to size-insensitive separation approaches in the field, with one of the goals being the isolation of rare cells such as circulating tumor cells (CTCs) from blood. Moreover, the project aimed to, ideally, establish an acoustic flow cytometer to phenotype single cells based on their cell-intrinsic acousto-mechanical properties and classify them in a label-free format based on differences or changes in their molecular and architectural structure.

During my work, I was engaged with several topics, including microfluidics, blood, cancer cells, and biophysical properties of cells; in this chapter, I provide a brief background knowledge for each. This chapter ends with the structure of the thesis.

1.1 From Macro to Micro

There are several motivations behind scaling down standard biochemistry laboratory settings by a factor of 10^3 or more to the tens-of-micrometers scale. One obvious advantage is that it significantly reduces the amount of required samples and reagents. Such linear decrease by a factor of 10^3 amounts to a volume reduction by a factor of 10^9, equips micro-scale devices to easily handle samples as small as 1 nanoliter (nl) or 1 picoliter (pl). In contrast, macro-scale devices need to process large samples with a volume of 1 liter (l) or 1 milliliter (ml). Small volumes become essential when there is no access to large samples and reagents, and analysis demands high detection efficiency and a short response time. Moreover, using small volumes offers compact and portable systems that can potentially grow for more adventurous bio/chemical handling and analysis systems such as deep space exploration (see MicroTAS 2023 program, plenary speaker Artur Chmielewski [1]). Finally, since the cost always matters, migrating to micro-devices may, in the long run, provide cheap setups for some applications.[2]

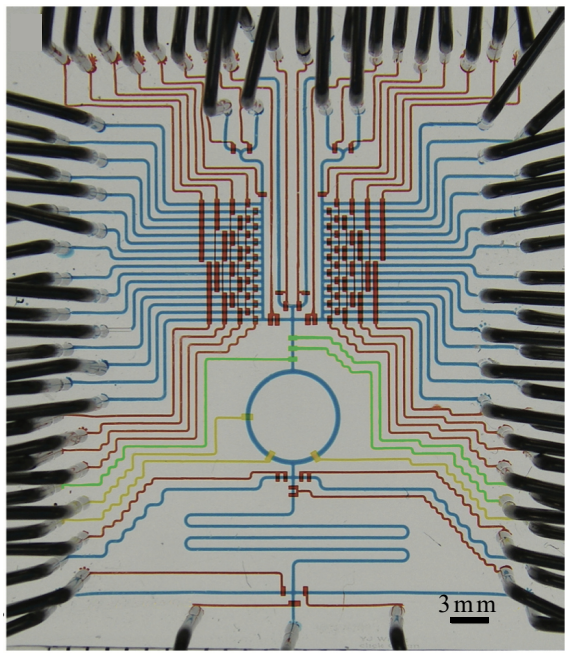

Figure 1.1: A microreactor equipped with 2 × 16 separately controlled reagent inlets (blue) designed for chemical reactions. Adapted with permission from Wang *et al.* [3].

In the realm of micro-scale devices, the science and technology of systems that deal with small volumes of fluids confined with channels of dimensions ranging from ten to hundreds of micrometers are called microfluidics. In his highly cited paper [4], George M. Whitesides introduced *four parents* for the field of microfluidics: molecular analysis, biodefence, molecular biology, and microelectronics. Microanalytical methods such as gas-phase chromatography, high-pressure liquid chromatography, and capillary electrophoresis, combined with optical detection schemes, shifted the paradigm of chemical analysis toward high sensitivity and resolution using tiny samples. With that advancement, it was inevitable to think of more compact and versatile versions of those methods for new applications in biochemistry. The second driving force of microfluidic systems lies in a series of programs in the 1990s supported by the Defense Advanced Research Projects Agency (DARPA) of the US Department of Defense. The program was designed to develop field-deployable microfluidic systems to detect chemical and biological threats. With the explosion of genomics and the advent of various areas of microanalysis in molecular biology, microfluidics became highlighted as a tool to increase the throughput. The fourth contribution to microfluidics stems from the fact that successful photolithography and associated technologies in microelectromechanical systems (MEMS) were applied to microfluidics.[4] Although, at the time, silicon and glass were used in fluidic microsystems, microfluidic expansion was caused by implementing a polymer called poly(dimethylsiloxane), or PDMS [5].

In the last decade, microfluidics has been established as a distinct new field and seems to have the potential to influence different subject areas, including point-of-care devices that provide affordable and fast diagnostics in regions with no access to conventional laboratories [6], [7], organ-on-a-chip devices for personalized drug testing on artificial human organs [8], microreactors shown in Fig. 1.1, where numerous chemical reactions can be quickly assessed in parallel and under different conditions [3], environmental monitoring such as exploration in soil [9], and related to the scope of this thesis blood fractionation to gain access to different cell types [10].

1.2 Blood

An average human adult has around 6-8 liters of blood (7-8% of total body weight) that runs through the veins, arteries, and capillaries. This fantastic body fluid has many different tasks while circulating, including transferring cells that are critical in the immune system, transporting oxygen and nutrients to the lungs and tissues, forming blood clots to stop bleeding, and regulating body temperature, among all other vital functions. Blood is a mixture of about 55% plasma, the liquid component of the blood, and 45% blood cells. In addition to water (90%), the rest of the plasma contains dissolved elements

such as carbohydrates, proteins, lipids, electrolytes, vitamins, and minerals, making it approximately 25 kg/m^3 denser than water. Blood cells are divided into three groups: red blood cells, white blood cells, and platelets [Fig. 1.2].[11]

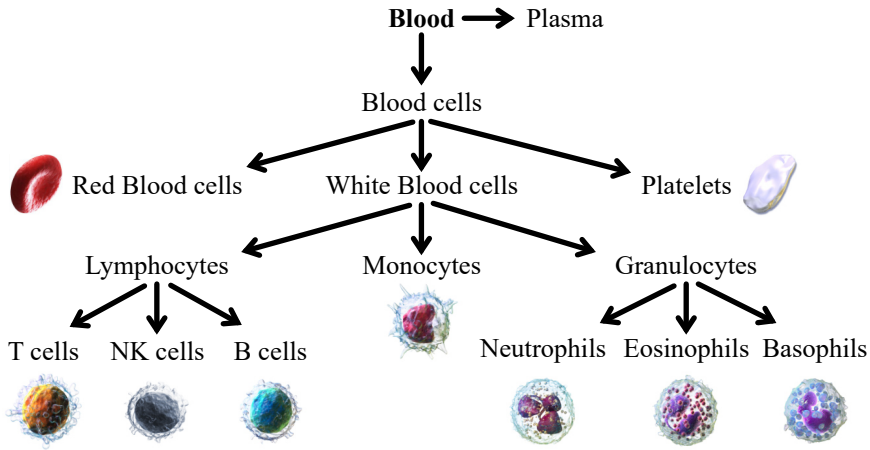

Figure 1.2: An overview of the composition of human blood, along with the breakdown of different types of blood cells [12], [13]. Pictures are adapted with permission from Blausen.com [14].

Red Blood Cells

Red blood cells, also called erythrocytes (RBCs), are the most abundant cell types found in the bloodstream and account for typically about 40-45% of blood. The volume fraction of RBCs in the blood, termed hematocrit (HCT), is a standard measure of RBC level and varies slightly among women and men. Their primary function is to carry oxygen from the lungs to the cells and return carbon dioxide to the lungs for exhalation. They are highly deformable since they do not have a nucleus; therefore, they can squeeze through small capillaries within the vascular system.[11]

White Blood Cells

White blood cells, also known as leukocytes (WBCs), are responsible within the immune system for protecting the body against all kinds of foes, such as infections and microorganisms. These cells consist of three classes: *lymphocytes*, *monocytes*, and *granulocytes*, all with different missions when the immune system asks. *Lymphocytes* constitute 20-25% of the WBCs population and are

prepared to identify specific antigens carried by pathogens upon their activation. T-cells, B-cells, and natural killer cells (NK cells) are three subtypes of *lymphocytes*. *Monocytes* originate from the bone marrow and are roughly the largest type of WBCs. They hold a 3-8% share of the WBCs population and differentiate into macrophages and dendritic cells. *Granulocytes* are the most abundant type of WBCs, with 60-70%, and are distinguished by the presence of granules within their cytoplasm. When the immune system calls, *granulocytes* protect the body against foreign invasion by releasing enzymes or toxins to eliminate specific target cells. *Granulocytes* include three types of cells: *neutrophils*, *eosinophils*, and *basophils*. Among these three, *neutrophils* stand out due to their high abundance (95% of the *granulocyte* population) and their involvement against bacterial and fungal infection.[15]

Platelets

Platelets or thrombocytes engage at the site of a vascular injury by clumping, thereby initiating a blood clot. These disc-shaped fragments have no cell nucleus and are produced in the cytoplasm of megakaryocytes [11]. In the event of vascular injury, *platelets* undergo three steps adhesion, activation, and aggregation. First, they attach to substances outside the disrupted endothelial layer. Second, they change shape, activate receptors, and release chemical signals. Lastly, they adhere to each other through receptor bridges and create a platelet plug.[16]

1.3 Cancer

Cancer stands as the second leading cause of death worldwide. It is estimated that the toll of cancer-related death to reach 13 million in 2030 [17]. However, according to the World Health Organization (WHO), around 30% of these deaths can be averted if patients receive early diagnosis and follow-up treatments before metastasis occurs [18]. Metastasis or migration of cancer cells is a process in which cancer cells intravasate from the primary tumor into the blood or lymphatic vessels and eventually extravasate into tissue and establish a secondary tumor [Fig. 1.3]. Although only 0.001–0.02% of cancer cells break into the peripheral blood, successful metastasis is believed to be responsible for about 90% of cancer-related deaths [19], [20].

Circulating Tumor Cells

The cancer cells released into the bloodstream from primary or secondary tumor locations are called circulating tumor cells (CTCs). CTCs were first discovered by Ashworth [21] in 1869, but their critical role in cancer biology has only

recently been emphasized [22]. This delay stems from the challenges tied to reliable CTC detection and separation, given that their occurrence is infrequent. With the current methods, it has been found that often < 100 CTCs exist per 10×10^6 leukocytes and 5×10^9 erythrocytes in 1 ml whole blood [23]. Over the last two decades, CTCs have been utilized as a liquid biopsy to monitor patients after treatment and have become complementary to tissue biopsies. Further investigation into these cells can advance our understanding of the metastatic process, tumor evolution, heterogeneity, and resistance to therapy [24]. Nevertheless, isolation of CTCs is technically difficult, mainly due to their rarity among a high background of blood cells. Furthermore, their isolation is challenging due to the following factors: (i) similar morphology to some WBCs, (ii) phenotypic heterogeneity which results from the epithelial-to-mesenchymal transition (EMT) that limits the use of biomarker-based separations, and (iii) maintaining their integrity for subsequent analysis.[25]

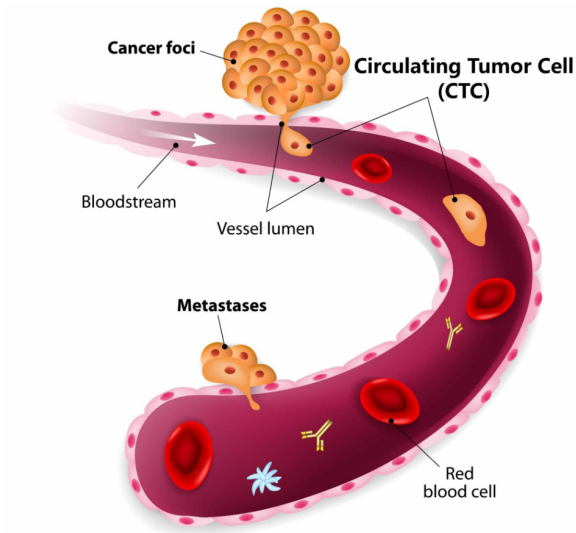

Figure 1.3: Dissemination of cancer cells from the primary tumor into the bloodstream. CTCs that manage to survive in the bloodstream may exit the circulation and form secondary tumors. Picture is taken with permission from Vycap.com [26].

The CellSearch System (Janssen Diagnostics) is the only medical instrument in the market approved by the US Food and Drug Administration (FDA) in 2004 for CTC isolation and enumeration. Despite being used in many labs and clinical studies, it has become increasingly evident that this standard method to isolate and classify CTCs by magnetizing them through specific chemical labels is biased and fails to find CTCs in many cases [27], [28]. Hence, there is a strong motivation for a sophisticated cell isolation method that provides fast

and efficient separation of CTCs for downstream analysis.

Cancer Cell Lines

Cancer cells here refer to both immortalized cell lines and primary cancer cells. Cancer cell lines (derived from primary cancer cells in the first place) are immortalized to divide and grow under controlled laboratory conditions continuously; however, primary cancer cells are extracted directly from cancerous tissue for in vitro experiments [29]. Unlike cancer cell lines, primary cancer cells can not proliferate indefinitely within a lab environment. Moreover, they are more biologically representative of the original tumor. The critical difference between the immortal cancer cell line and primary cancer cells is their genetic composition. Cancer involves genomic instability, and most primary tumors express substantial heterogeneity due to their subclonal nature [30]. In contrast, immortalized cancer cell lines are derived from a single clone and lack heterogeneous characteristics; that is, they can not entirely represent the accurate response of cancer to treatment and therapies for different patients since they originated from one individual. Despite the potential drawbacks, they are invaluable biological tools and have enabled many significant breakthroughs in oncology research. Some of their advantages are relatively inexpensive with less maintenance compared to animal models, easy to grow indefinitely and store, and highly reproducible results.[29] The results presented in the included Papers of this thesis are produced based on immortalized cancer cell lines. For example, Jurkat (clone E6-1) is a clone of the Jurkat-FHCRC cell line, a derivative of the Jurkat cell line established from the peripheral blood of a 14-year-old male acute T-cell leukemia patient.

1.4 Biophysical Properties of Cells

Phenotyping of single cells based on their intrinsic biophysical properties, such as their size, is already a tool for classifying cells. The Coulter counter measures the resistance of a small aperture while a cell passes through and correlates the resistance changes to cell volume [31]. More specific classifications can be done based on differences or even changes in their molecular and architectural structure. Thanks to microfluidics, high-throughput biophysical phenotypes of cells (e.g., cell morphology, mass, or stiffness) nowadays can be probed in a label-free format, minimizing laborious and costly experimental protocols. One obvious advantage of accurately charting the biophysical signatures of cells is that the separation outcome improves drastically. Over the past decade, biophysical cytometry has been developed mainly within four phenotypes: electrical, optical, morphological, and mechanical (Table 1.1). Membrane capacitance and cytoplasm conductivity mainly define the electrical phenotype of cells and have

been used to characterize and discriminate cell types (e.g., stem cells, blood cells, cancer cells, and microbes) through microfluidic impedance flow cytometry [32]–[34]. Label-free imaging modalities have been developed for blood diagnostics [35], [36]. Even bright and dark-field textures of cells can provide rich information about their intrinsic morphologies and classify immune cell subtypes [37]–[39]. For more information on the details of each technique for biophysical cytometry and their applications, the reader is referred to Refs. [31], [40]–[42].

Table 1.1: Summary of state-of-the-art biophysical properties. Adapted with changes from Lee *et al.* [40]

Phenotype Class	**Biophysical Property**
Electrical	Cytoplasm resistivity
	Cytoplasm conductivity
	Membrane capacitance
	Specific membrane capacitance
Optical	Absorption
	Scattering
Morphological	Shape/Size/Volume
	Intensity
	Texture
	Temporal
Mechanical	Mass
	Density
	Deformation
	Stiffness
	Compressibility
	Adhesive force
	Traction force

Mechanical phenotypes include mass, density, deformation, stiffness, compressibility, and adhesive and traction forces. Among them, the density and compressibility are crucial to this thesis, and the acoustic properties of cells and have been mentioned in all the included Papers. Live-cell mass assays have been studied using microelectromechanical systems (MEMS)-based microfluidic devices and quantitative phase imaging [43], [44]. Among them, the suspended microchannel resonator (SMR) stands out and offers extraordinary sensitivity to measure the suspended cell's mass (down to femtograms) and density during the growth cycle [45]–[47]. The buoyant density of cells has been measured with different methods, such as density gradient centrifugation [48], particle tracking [49], and Refractive index tomography [50]. Deforma-

bility cytometry [51], [52] at high speed (100-1000 cells/s) implements various configurations such as hydrodynamic stretching (inertia-dominated flow [53], [54] or shear-dominated flow [55], [56]) and micro-constriction [57], [58] to monitor time-dependent elastic mechanical properties. Compressibility of cells has been reported particularly within the acoustofluidics research field and can be seen as an additional parameter to more common measures of Young's and shear modulus of the cell. The last section of chapter 3 and Paper IV discuss charting the density and compressibility of cells in the acoustofluidics research field.

1.5 Motivation of the Thesis

Conventional techniques for target cell detection, such as flow cytometers, fluorescence scanning microscopy, and size-based filtration that I will introduce in the next chapter, mainly struggle with significant limitations, including the capacity to process large blood volume, cell loss, compromised viability, and clogging. Microfluidic techniques as alternative approaches to isolate these cells come into the picture. Microfluidics host two different general approaches for cell separation: affinity-binding (label-dependent) and label-free. Label-dependent methods work based on antibody-antigen interaction and are combined with magnetophoresis and nanostructures to improve the separation efficiency and recovery rate. One key benefit of the magnetophoretic separation over its macroscale counterpart (CellSearch System) is its continuous operation and higher throughput. To overcome some of the challenges in affinity-biding techniques, label-free methods based on the biophysical signature of cells have been developed extensively to enrich cancer cells [59].

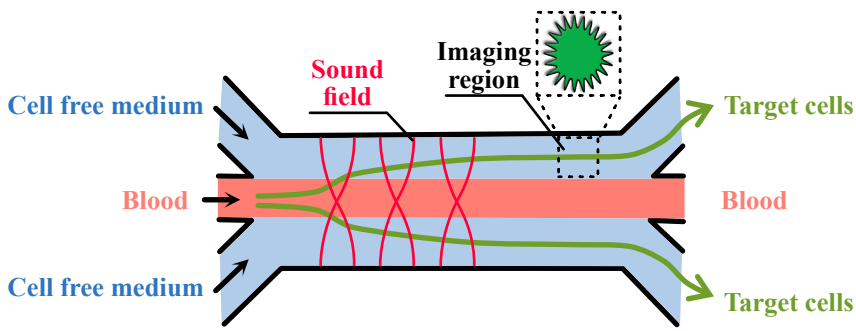

Figure 1.4: Conceptual schematic of isoacoustic focusing (IAF) to enable separation and imaging of target cells from blood. Illustration is reproduced with permission from Per Augustsson.

The vision of this project is to build an acoustic flow cytometer with applications, for instance, in cancer diagnostics. In such an instrument, rare disease-related cells can be detected, imaged, and isolated directly from blood [1.4]. As a label-free method, the work of this thesis aims to develop, characterize, and apply an enabling ultrasonic wave-based technology, isoacoustic focusing (IAF), to gain access to target cells in a phenotype-specific manner.

1.6 Structure of the Thesis

During the work of this thesis, a considerable effort was put into research resulting in four Papers as the main part. Papers I and II, with a reformatted version of the publications, and manuscripts III and IV are included in the second part of this thesis. Supplemental materials are included immediately after each Paper. The first part, overview of the research field, consists of six chapters and is intended to put the Papers into context by providing the background and context to the studies. The included chapters in the first part of this thesis are as follows:

Chapter 1 Introduction — Brief introduction to the main elements and the motivation for the research in this thesis in a broad perspective.

Chapter 2 Cell Separation Methods — Background on some of the most highlighted cell separation techniques both in macro and micro-scale.

Chapter 3 Acoustofluidics — Background on acoustofluidics including experimental model system, resonances, acoustic radiation force, acoustic streaming, acoustophoretic particle and cell trajectories, and challenges in acoustophoresis.

Chapter 4 Isoacoustic Focusing — Introduction to isoacoustic focusing (IAF), acoustic body force, suppression of acoustic streaming, and some of the practical considerations.

Chapter 5 Summary of the Included Papers — Brief summaries of the motivation and the main results of each of the included Papers I, II, III, and IV.

Chapter 6 Conclusions and Outlook — Conclusion of the thesis and outlook with suggestions for future research.

Chapter 2

Cell Separation Methods

In biomedical research and clinical laboratories, isolating specific cell types from complex biofluids and heterogeneous cell mixtures is often necessary for further analysis, whereby preserving cell viability and function is essential. Enabling technologies that can purify subgroups of cells from the blood within minutes are therefore sought to facilitate lab work and inline integration with high-end bioanalytical instrumentation. The difficulty as mentioned briefly in the previous chapter, is that blood is an extremely diverse and crowded suspension of cells and particles, and about 40% of the blood volume consists of red blood cells (RBCs). This makes it challenging and time-consuming to isolate rare species from the blood, such as white blood cells (WBCs), circulating tumor cells (CTCs), or sub-micron particles such as exosomes or bacteria.[60] Moreover, to shorten the time from sampling to result, there is an interest in shifting from analysis in centralized labs to point-of-care tests and patient self-testing for increasingly more advanced tests [61].

This chapter addresses the need for the above-mentioned methods first at the macroscale by reviewing the most common techniques that the author also used during the work of this thesis. The rest of this chapter is dedicated to the most highlighted microscale methods and, in particular, label-free devices with a few examples. The ultimate goal of this thesis is to provide a better separation outcome for target cells, particularly in Paper III, where We enrich peripheral mononuclear cells (PBMCs) from whole blood; therefore, it is necessary to compare to other techniques in terms of the performance of the device. The content of this chapter is inspired by some of the previous Ph.D. theses in the acoustofluidics research group at the Department of Biomedical Engineering [62]–[64].

2.1 Macroscale Methods

Macroscale or traditional platforms for cell isolation are firmly established in biotechnology for different assignments such as cell preparation, processing, and isolation. They serve as gold-standard techniques, and what they offer in terms of labor intensity, cost, and complexity varies. Their performance parameters, including throughput, sensitivity, and efficiency, are not the same. Well-known techniques to fractionate blood rely on selective lysis, centrifugation, and molecular labels, and typically cells are exposed to a series of lengthy procedures such as repeated washing and resuspension, and incubation with labels. Among the conventional methods [Fig. 2.1], centrifugation, magnetic-activated cell sorting (MACS), and fluorescence-activated cell sorting (FACS) are inevitable choices and will be briefly introduced in the following.

2.1.1 Centrifugation

The gravitational force causes micro-objects that are denser than the carrier liquid to sink down in a container. The micro-objects' size and difference in density relative to the surrounding media determine the sedimentation rate. In our context, a blood sample separates over time in a test tube under gravity alone. RBCs are heavier compared to the other elements and simply descend into the bottom of a collection tube. Lastly, the plasma stays upper in the tube with no RBC in it [65]. Centrifugation is an expedited version of this slow process and offers a simple procedure, low cost, and the capability to process large numbers of cells [Fig.2.1(a)]. Centrifugation parameters such as time and speed enable selective control over the outcome. For instance, the correct choice of speed and time determines whether platelets are separated from plasma or retained [66]. A sequence of centrifugations, referred to as differential centrifugation, presents another approach to divide the same sample further in order to isolate the target cell type. In this approach, after each step, the pellet is removed, and the speed increased until the smaller cells are separated. This strategy is commonly implemented in platelet preparations [67]. Nevertheless, it has limitations such as low resolution, compromised purity, and the potential for loss of target cells, especially when samples have low cell counts or small volumes.

Density gradient centrifugation improves the separation resolution and efficiency to some extent [68]. In this version of centrifugation, cells initially sit on top of a separation medium incorporating gradual change in the density by using substances such as Ficoll [69], Percoll [70], [71], Optiprep containing iodixanol [72], or other gradient media (e.g., based on polysaccharides and silica particles). When centrifugation starts, cells sediment through layers of liquids of different densities formed by the gradient media until they reach their neutral buoyancy points. This equilibrium position is called the isopycnic point.

In Paper IV, We have developed a module to generate linear, continuous, and highly reproducible density gradients of different ranges by mixing iodixanol and phosphate-buffered saline (PBS) to gain access to cells' density based on their location in the gradient.

Although density gradient centrifugation finds extensive application in mononuclear cell isolation from whole blood and bone marrow samples [73]–[75], drawbacks with this method are that (i) the accuracy is limited by the difficulties of accurately collecting the thin sheaths of layered cells from the test tube for cells of contiguous densities, (ii) it can not easily be implemented for applications of handling small sample volumes, and (iii) it is challenging to implement in a flow-through format for in-line integration in compact automated analytical instrumentation to facilitate diagnosis or treatment of a patient at the point-of-care.

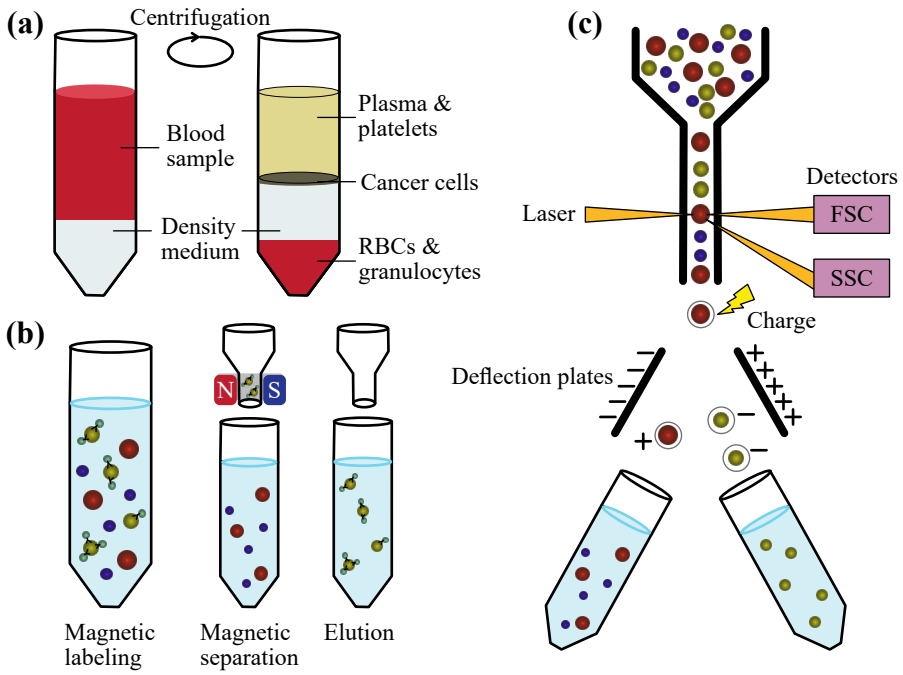

Figure 2.1: Schematic illustration of (a) density gradient centrifugation of blood, (b) magnetic-activated cell sorting, and (c) fluorescence-activated cell sorting. Illustrations are reproduced with permission from Ref. [63].

2.1.2 Magnetic-activated Cell Sorting (MACS)

Miltenyi Biotech first launched magnetic sorting and registered it as the trademark MACS [76], [77]. MACS operates based on the affinity-based binding of antibody-conjugated magnetic beads to cells. This allows cells to retain in the magnetic field while unlabeled cells flow through the separation chamber [Fig. 2.1(b)]. Due to its high throughput, reasonable purity, and availability of magnetic particles in many conjugations, this technique is well-established in research and clinical applications. Additionally, biodegradable magnetic beads (∼50 nm size) are accessible to ensure no interference of attached particles in downstream analysis [76]. In positive selection [78]–[80], magnetic beads are bound to the target cells' antigens (e.g., CD34+), whereas in negative selection, they are bound to non-target cells for selective cell depletion. Negative selection, for instance, has been used to remove CTCs [81], [82] or other unwanted cells (such as CD3+ cells) from the cell product [83]. Throughout the work of this thesis, neutrophils and peripheral mononuclear cells (lymphocytes and monocytes) were extracted directly from blood using EasySep^{TM} Isolation Kit for the purpose of different experiments, which works based on negative selection.

MACS is regarded as the gold standard in numerous biomedical and research applications. Nevertheless, it relies on a specific cell marker and typically targets only one surface antigen in each operation, and it has been shown in some cases that it can potentially impact cell settings such as viability, proliferation, phenotype, activity, and function. [84]–[86]

2.1.3 Fluorescence-activated Cell Sorting (FACS)

The concept of FACS was first documented in 1972 [87]. Multiparameter optical set-up in the flow cytometer enables analysis and classification of single and even rare cells in suspensions based on their specific light scatter or surface maker profile. First, each cell hydrodynamically focused in a narrow stream passes the optical interrogation points in the flow chamber. Second, the optical detectors in the system detect scattered light and fluorescent signals (generated by different lasers) for each cell and assign a specific signature. After this, each cell becomes trapped in a droplet, and each droplet acquires a charge accordingly. Finally, an electrostatic deflection system navigates droplets into separate collection tubes [Fig. 2.1(c)] [88], [89]. In Paper III, We analyzed cell samples by BD FACS Canto II flow cytometer (BD Bioscience) to evaluate the separation efficiency of peripheral mononuclear cells (PBMCs) from undiluted blood.

FACS machines can achieve a very high event rate depending on the machine and application, and they offer high purity for clinical cell analysis by labeling before the optical detection. Drawbacks are that cells are sorted in sequence,

limiting the throughput to ∼1000 total cells per second, and that the involved aerosols can spread pathogens [89]. It should be noted that pretreatment steps are typically required by manual centrifugation and pipetting efforts to stain and deplete unwanted cells. Some other considerations are that the equipment, material, maintenance, and reagent are costly, and the instrumentation requires sufficient training.

2.2 Microscale Methods

In microfluidics, as mentioned previously, there are excellent capabilities to control fluids in confined volumes. The predictable behavior of fluids within microchannels and the ability to apply an external force field offer a wide range of opportunities for precisely manipulating fluids with suspended cells and microparticles. The manipulation regimes can be broadly divided into passive and active. Unlike most conventional methods, a lot of attention in microfluidics has been focused on achieving label-free separation of cells and particles based on distinction in their inherent biophysical properties such as size. There are a handful of microfluidic methods for cell separation, and the reader is encouraged to consider Refs. [90], [91] for more insight; however, this section reviews a few selected techniques that I think particularly show promising results.

2.2.1 Fluid Dynamics at the Microscale

In microfluidics, flow velocities generally fall within the low Raynolds number (Re) range ($\ll 2000$), where viscosity takes over while inertial effects become less important. In such circumstances, the flow in a microchannel maintains a laminar pattern [Fig. 2.2(a)]. The $\mathrm{Re} = \rho u L/\eta$ describes the ratio between fluid viscosity and inertial forces and predicts whether the fluid behavior is turbulent or laminar. In Re's formula, u, L, ρ, and η stand for fluid velocity, channel dimensions, fluid density, and dynamic viscosity, respectively. In a laminar flow regime, the velocity remains consistent over time, and the fluid moves smoothly and deterministic in the channel. As a result, particles or cells follow the pathways along which they were initially introduced to the microchannels, either if it is a random distribution of position or if they are pre-aligned in some way, such as by using external forces.

Due to the assumption of non-slip boundary condition at the channel walls for Newtonian fluids (aqueous, incompressible, uniform, and viscous), when the flow is steady and laminar, the fluid velocity is highest in the center of the channel and has its minimum (zero) at the sidewalls. This implies that the flow profile is parabolic, and it is known as the Poiseuille flow [Figs. 2.2(b) and (c)]. Consequently, suspended particles or cells experience different retention

times in the microchannel depending on their distance from the walls. When particles or cells move through viscous fluids as a response to an external force field in a microchannel, the well-known Stokes' drag force ($\boldsymbol{F}_{\text{drag}}$) comes into the equation. The drag force acts against the external force and limits the particle or cell velocity. Dynamic viscosity (η), the particle/cell radius (a), and the particle's velocity (u) determine this force, and We will cover it later in a section for particle/cell trajectories.

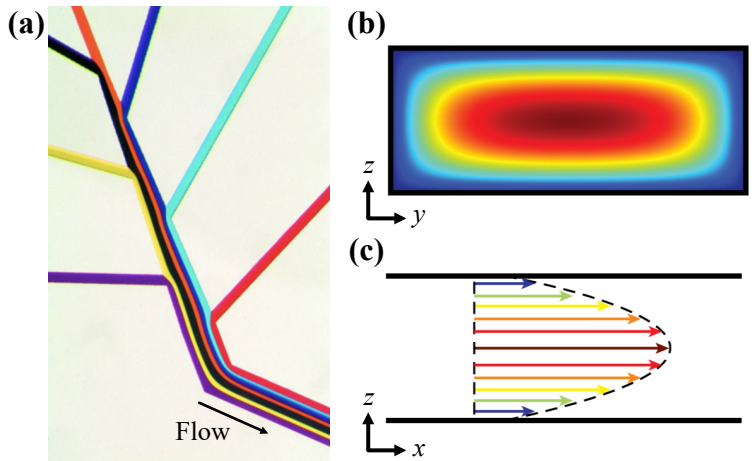

Figure 2.2: (a) An example of laminar flow in a microchannel [92]. Photo credit Felice Frankel. A typical parabolic flow profile is shown in (b) the cross-section and from (c) the side view. Due to the no-slip boundary condition, the fluid has its maximum velocity (red) in the center of the channel, and at the channel walls, it goes to zero (dark blue). Reproduced with permission from Ref. [62].

2.2.2 Passive Techniques

Microfluidic passive techniques separate particles/cells through interactions with the microchannel's structures, other particles/cells, or through lift and drag forces induced by the fluid flow. In such systems, the hydrodynamic forces generated in the microchannel alter the trajectories of the particles/cells, eventually focusing them towards the device outlet for separation purposes.

Filtration

One straightforward way to separate cells is based on size exclusion. Indeed, cell size serves as the key factor in cell separation methods, it is also mainly responsible for volume-based forces. Microfluidics allows filtration based on size

or deformability, for example, using membranes [Fig. 2.3(a)] is one common way. They typically operate in two modes: dead-end and cross-flow filtration [90]. In dead-end filtration, the feed flow is directed perpendicular to the membrane surfaces, while in cross-flow, it is parallel to the membrane. Microscale filtration has been adopted for applications including apheresis, blood component fractionation, and isolation of rare cells.[93]–[98] The advantages of this label-free approach are convenient handling, fast use, and flexibility, and they can serve as a pre-enrichment step. However, filters usually suffer from clogging when dealing with concentrated samples. Other issues associated with this technique are (i) cell size distributions often overlap or vary, and such fact makes it difficult to choose the right cut-off size, (ii) more deformable cells can principally squeeze through filter openings smaller than their diameter, (iii) more shear stress results in cell loss, activation, and damage.[99]–[102]. For more information on another regime of filtration called hydrodynamic filtration, the reader is referred to Refs. [103]–[106].

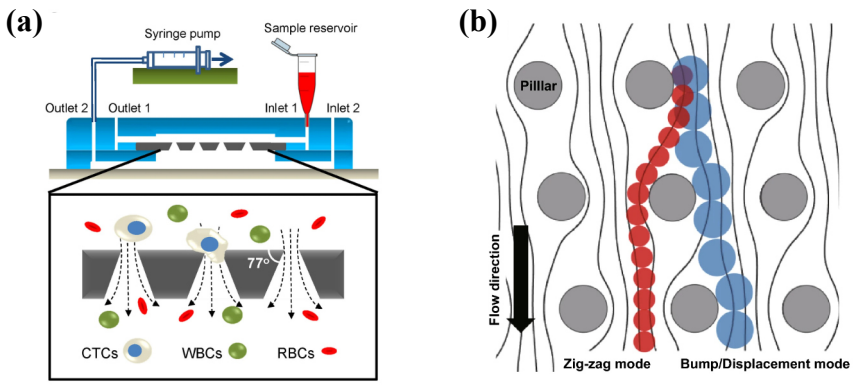

Figure 2.3: (a) Schematic illustration of the experimental setup for CTC filtration. The filter with conical holes is made of polyethylene glycol diacrylate (PEGDA) and placed between two patterned PDMS layers. A syringe pump of constant speed pulls the introduced sample from inlet 1 to outlet 2. Adapted from Tang *et al.* [107]. (b) Principle of DLD: particles with size smaller than the critical diameter follow a zigzag trajectory, while larger particles move in a bumping mode. Adapted from Salafi *et al.* [108].

Deterministic Lateral Displacement

Implanted microstructures inside a microchannel deflect the flow path and offer cell/particle separation based on size, density, and deformability. Various shapes and geometries (grooves and herringbones as examples, among others), planar or lateral to the flow, have been experimented to isolate, enumerate,

and concentrate cells/particles. These arrays also work well for lab-on-a-chip mixing applications [109]. They have been combined with other separation or (affinity-) capture methods to perform better. Despite pioneering CTC isolation, this approach is costly and challenging to fabricate. [110]–[114]

Deterministic lateral displacement (DLD) exploits micro-post arrays as implanted microstructures to hydrodynamically separate particles/cells with submicrometer resolution in continuous flow. In DLD, the structure of the arrays and size distribution of particles/cells determine particles/cells smaller than critical size stick to their streamline with no lateral moves. On the other hand, particles/cells above the critical diameter experience a sideways shift, causing them to migrate towards the adjacent streamlines [Fig. 2.3(b)]. This mechanism, as you can imagine, enables the collection of cell types based on their final position at the end of the array. DLD has been studied extensively for RBCs, WBCs, platelets, CTCs, and stem cells with a good size resolution. [115]–[123] In DLD, low flow rates are primarily associated with devices having a narrow height and this is typically due to difficulties in fabricating posts with high aspect ratio. The separation can be upscaled by employing multiple devices in parallel. Lastly, clogging, shear stress, damage, and platelet activation are the major issues associated with this technique. [124]–[126]

Inertial Focusing

Among passive microfluidic techniques for cell separation, inertia-based devices stand out by holding great potential for high-throughput standard cell processing applications, notably CTC isolation. Although at a low Reynolds number, the influence of inertial effects is negligible, these microfluidic setups function at higher flow rates (Re 1-100), where inertial effects become significant. [127] This technique, similar to previous ones, exploits size, deformability, and shape for cell separation. Inertial focusing brings into service the balance between two inertial lift forces, the wall effect lift, and the shear gradient lift force. The equilibrium locations of particles/cells at the end of the device depend on the channel dimensions and geometry. In the case of spiral or asymmetrically curved channels, another inertial effect, the Dean flow, comes into play [Fig. 2.4]. Drag force from the Dean flow balances with the lift forces and results in size-dependent positioning of particles in the cross-section of the microchannel and has been extensively explored in blood fractionation and rare cell isolation[128]–[135]. Inertial systems do not need external force fields and operate with relatively simple laboratory setups, but they often require a substantial dilution of samples such as blood. These devices are application-specific, that is, a new application often demands a precise configuration of channel dimensions, which must be calculated and tested.[136]–[143]

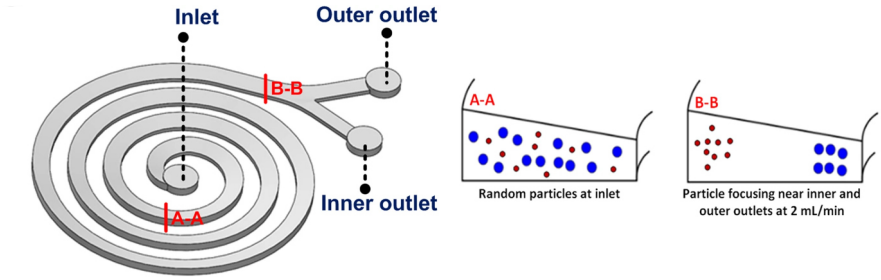

Figure 2.4: Inertial cell separation in spiral channels: within trapezoidal cross-section and curved channels, the final equilibrium position of particles/cells with respect to the walls is responsible for the separation outcome. The size and contribution of lift forces and Dean drag forces determine the final location. The lift forces direct them towards the inner walls, and the Dean drag forces push them towards the outer wall. Adapted from Warkiani *et al.* [144].

2.2.3 Active Techniques

In active techniques, particles/cells undergo separation by interaction with the microchannel structure and an externally applied field. The introduced force field alters the motion of particles/cells relative to the flow, resulting in focused trajectories in particular locations of the channel cross-section. Compared to passive approaches, active devices are often more flexible in their applications since they can host different sizes or types of particles without redesigning the device, and they may be more complex to fabricate.[91]

Magnetophoresis

Magnetophoresis exploits the cell's intrinsic magnetic susceptibility to separate paramagnetic RBCs (based on hemoglobin oxygenation levels) and diamagnetic WBCs in magnetic fields [145], [146]. Due to the limited presence of innate magnetic properties in different cell types, affinity-based magnetophoresis has been developed. This involves binding magnetic particles to target cells, enabling continuous flow separation in microdevices featuring built-in magnetic fields. A non-uniform magnetic field deflects magnetic particles perpendicular to the fluid flow [Fig. 2.5(a)], whereas non-labeled cells remain unaffected and follow the streamlines. Beads with different magnetic characterization facilitate even multiplex separation of rare cells and bacteria.[147]–[152]

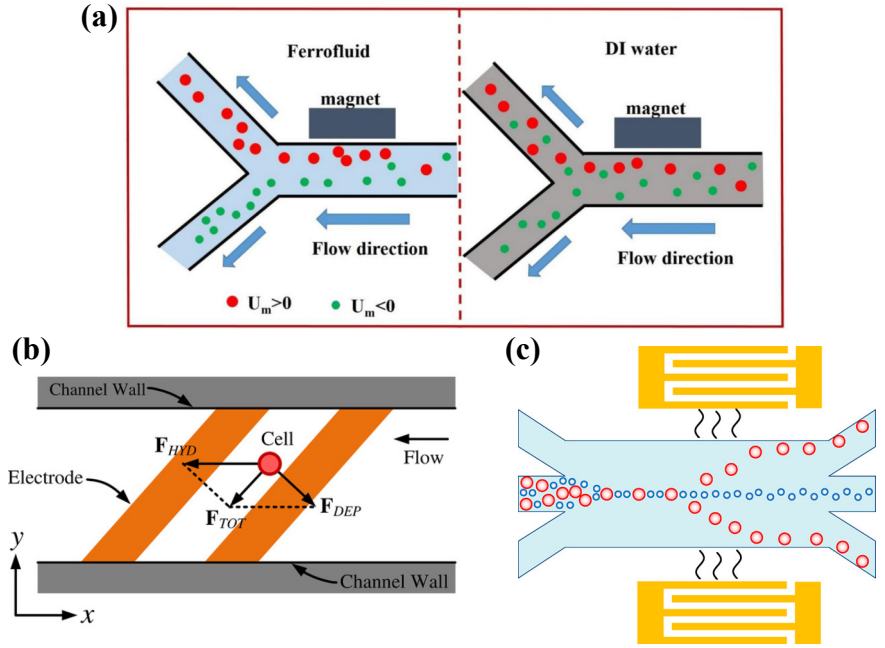

Figure 2.5: A Few examples of microfluidic active techniques for cell separation. (a) The principle of the separation of magnetic and diamagnetic particles in ferrofluid and deionized (DI) water. Magnetic and diamagnetic particles are under the influence of positive ($\mathbf{U}_\mathrm{m} > 0$) and negative ($\mathbf{U}_\mathrm{m} < 0$) magnetophoresis, respectively. Adapted from Jiang *et al.* [153]. (b) Overview of the forces acting on a cell at electrodes. The pDEP in this configuration is sufficiently strong to deflect the cells along the electrode edge towards the channel wall. Adapted from Techaumnat *et al.* [154]. (c) Schematic illustration of microfluidic particle separation using a SSAW field. Particles of different sizes are first focused to the center of the channel by two side streams, and then the SSAW field is produced by two interdigital transducers (IDTs) positioned on opposing sides of the channel. Finally, due to the size-dependent acoustic radiation force, particles experiencing different lateral displacements lead to separation in the outlet. Adapted from Ai *et al.* [155].

Dielectrophoresis

In dielectrophoresis (DEP), the size and the dielectric signature of cells relative to the suspending fluid are the key parameters. Particles/cells suspended in a non-uniform DEP force field encounter forces (positive or negative) due to an induced or permanent dipole. Factors such as applied voltage (AC or DC), frequency, and electrode geometry determine the field strength. Positive DEP

(pDEP) directs more polarizable particles/cells toward the strong part of the field, while nDEP does the opposite to the less polarizable particles/cells [Fig. 2.5(b)]. DEP operates both in continuous flow format and batch mode to capture target cells and remove undesirable ones in different contexts, including CTC isolation, stem cell enrichment, and cell cycle synchronization.[156]–[164]

Acoustophoresis

Acoustophresis employs an acoustic pressure field in microchannels to manipulate particles/cells based on their acoustic properties. Size, density, and compressibility relative to the carrier liquid represent the acoustic properties. Acoustophoresis has been proven to be a gentle way of handling cells with no observable alterations in viability, proliferation, DNA damage, or function [165]–[167]. Like in medical imaging ultrasound, these acoustic separation modules typically operate at frequencies above 1 MHz where cavitation is minimal (in contrast, sonicators ($\sim$20 kHz) are commonly used to disrupt the cell membrane). While flowing through the separator, each cell experiences approximately 0.1 s of exposure to sound, and this causes a sideways translation on the order of $\sim$0.1 mm. Near the end of the separator, the cells congregate in a pressure node and are never in direct contact with the resonator walls. Even sensitive cells, such as neurons and glial cells, have been processed in microchannel acoustophoresis with no observed damage [165]. The exerted forces on cells in this context are comparable in magnitude to centrifugation with the clear benefit of being straightforwardly implemented for in-line processing at, currently, up to 10 milliliters per minute flow [96], [168]–[171].

Table 2.1: Comparison of different acoustophoresis techniques. Adapted from Ref. [91].

Type	**Advantages**	**Disadvantages**
BAW	Simple device architectures, high throughput	Difficulties in handling nanoparticles, heat generation
SSAW	High precision, easy to miniaturize, strong acoustic radiation force	Low throughput
TSAW	High precision, easy to miniaturize, single IDT required	Low throughput, design consideration to prevent formation of standing wave

The two major forms of acoustic micro-devices (Table 2.1) are based on bulk acoustic waves (BAW) and surface acoustic waves (SAW). BAW systems typically operate at high throughput compared to SAW devices. They effi-

ciently provide a standing half-wave acoustic field and require rigid material attached to actuating piezoceramic transducers (PZTs). On the other hand, SAW devices using standing (SSAW) or traveling (TSAW) surface acoustic waves are often built with polymers such as polydimethylsiloxane and exploit interdigitated transducers (IDTs) for sound propagation [172]. In these chips, the operation of IDTs at high frequencies enables accurate manipulation of particles/cells, albeit at modest throughputs [Fig. 2.5(c)]. SAW devices with excellent promise for diagnostics and point-of-care applications have been investigated for cell washing and concentration, bacteria, and CTC isolation.[173]–[177] The work of this thesis deals with a BAW device which will be covered in detail in the next chapter.

2.3 Concluding Remarks

With the current benchmark isolation methods, cells are exposed to a series of lengthy procedures that, in practice, delay the final analysis. Microfluidics as an alternative provides opportunities to replace some of the standard methods to reduce the overall processing time and manual interventions by performing label-free and in-line purification and analysis of various bioparticles such as cells, pathogens, and extracellular vesicles in their unbiased state. Over the last 20 years, more than 100,000 articles about microfluidic particle/cell separation have been published [91], showing that this area is of great interest to researchers, and further developments are expected. Nevertheless, to fulfill the requirements for a specific application, such as high specificity and simple operation for medical diagnostics devices, many challenges have still to be solved. In that regard, the work of this thesis addresses some of the challenges in BAW devices for cell characterization and separation.

Chapter 3

Acoustofluidics

Acoustofluidics represents a combination of acoustics and fluid dynamics. The field has received increasing attention in recent decades due to its promising applications in biomedical and lab-on-a-chip devices and the ability to generate strong forces at the microscale. As a comprehensive overview of the field, the Lab on a Chip journal in 2012 published a themed collection on acoustofluidics for particle or cell manipulation with 11 articles. This tutorial series now includes 24 articles [178] covering theory and experiments, aiming to demystify this growing field and provide a unified perspective for users. The capabilities of acoustofluidic technologies span a spectrum of applications, including the patterning of heterogeneous cells for tissue engineering and automated isolation of bioparticles from body fluids for faster and personalized patient treatment.[179], [180] One fundamental concept in acoustofluidics is to use sound to translate particles or cells, commonly called acoustophoresis. The first appearance of this term to describe active manipulation of particles within microfluidics is found in a U.S. patent detailing a device for separating species via acoustic waves. This patent was filed in 1992 and was attributed to the United States National Aeronautics and Space Administration (NASA) [181], [182].

This chapter aims to provide a background for microchannel acoustophoresis and describe the phenomena essential for understanding the acoustophoretic motion of particles/cells. The chapter starts by introducing the experimental model system and ends with a section explaining the current challenges in the field for both cell separation and cytometry applications. The theoretical content provided in the current chapter basically owes its existence to the Ph.D. theses of Per Augustsson [183], Rune Barnkob [184], and Jonas Karlsen [185].

3.1 Experimental Model System

The experimental acoustophoresis model system in the work of this thesis represents a class of hard-material acoustic devices for the generation of bulk acoustic resonances in the presence of homogeneous media. The core of such a device is a silicon/glass microchip attached to a piezoelectric transducer (piezo) that generates ultrasound vibrations. For more description of the realization of acoustophoresis devices, the reader is referred to article 5 in the acoustofluidics tutorial series [186].

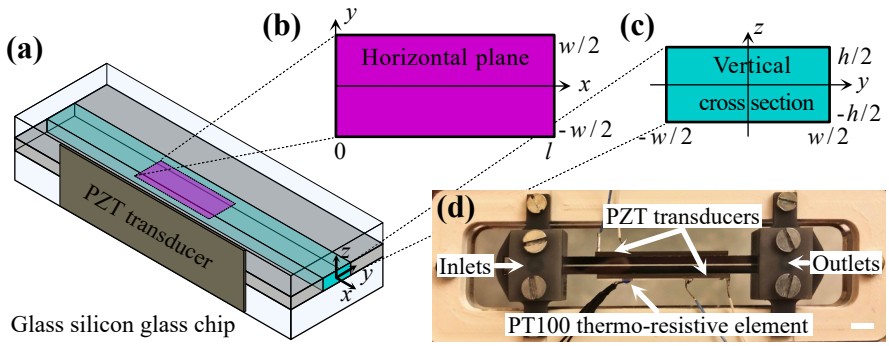

Figure 3.1: Experimental acoustophoresis model system. (a) Illustration of a section of the acoustophoresis chip of size $L \times W$ with an etched microchannel of width w and height h. The silicon (gray) is sandwiched between two glass lids (transparent gray) of thickness 500 μm and 610 μm. (b) Horizontal xy plane section (magenta) at the channel mid-height $z = 0$ of dimension $l \times w$. (c) Vertical yz microchannel cross section (cyan) of dimension $w \times h$. (d) A photograph of the chip placed in its holder. Scale bar is 5 mm.

The experimental model system [Fig. 3.1] consists of a glass-silicon-glass microchip (gray and transparent gray) with a length of $L = 70$ mm and width of $W = 4$ mm, which incorporates an etched microchannel to host particle/cell suspension via tubing connected to the inlets. The microchannel (cyan) of width $w = 375$ μm and height $h = 150$ μm is anodically bonded between two glass lids of thickness 500 μm and 610 μm [Fig. 3.1(a)]. The piezo of the type Pz26 from Ferroperm Piezoceramics, Denmark, is glued to the side of the chip and typically has a size of 30 mm $\times$ 4 mm $\times$ 1 mm. In this context, the orientation is defined as follows: x always points along the channel length, y across the channel width, and z along the channel height. In Fig. 3.1(b), the horizontal xy plane (magenta) of dimension $l \times w$ is shown. The plane is positioned at the channel mid-height $z = 0$, and the length l refers to the length of a given microscope field of view. Figures 3.1(c) and (d) show the vertical yz

microchannel cross section (cyan) of dimension $w \times h$ and a photograph of the chip placed in its holder. A PT100 thermo-resistive element was always used to monitor the temperature on the piezoceramic transducers (PZTs).

3.2 Resonances

It is essential to establish an acoustic resonance to achieve a sufficient acoustic energy density to manipulate particles/cells in a carrier fluid. In the resonant field, the frequency of the acoustic transducer fulfills the condition that the channel width should be a multiple of half the acoustic wavelength. The resonances in the microchip rely on several factors, such as piezo actuation, glue layer attaching the piezo to the microchip, mechanical loading of the piezo and the chip, and channel materials and geometries. Here, We employ a basic model to explain the resonances inside the liquid-filled microchannel. To achieve that, the potential interactions with the bulk chip and the spatial behavior of the piezo actuation are disregarded.

From a mathematical perspective, resonance signifies a system entering its eigenmodes, where the acoustic energy density becomes unbounded. However, when small losses are present, the energy density remains bounded but very large compared to the vibration source.

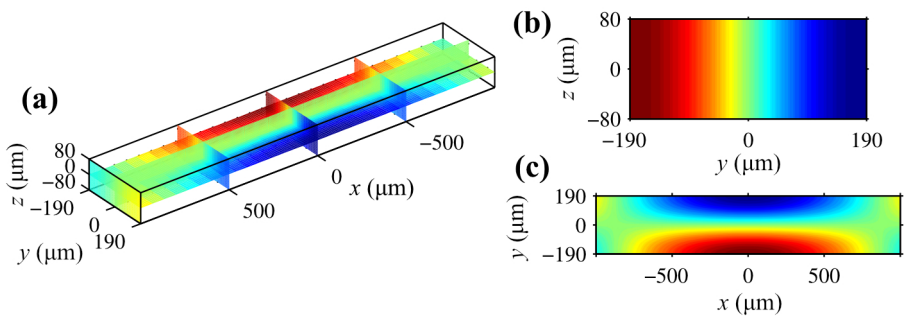

Figure 3.2: Pressure eigenmode p_1, which ranges from p_a (dark red) to $-p_a$ as described by Eq. (3.4), for a liquid rectangular cuboid surrounded by hard walls. The input dimensions are similar to the microchannel in the experimental model system, Fig. 3.1. The eigenmode is characterized by $(n_x, n_y, n_z) = (20, 1, 0)$, and only the portion of the channel extending 2 mm around $x = 0$ is shown. (a) Three-dimensional slice plot of the eigenmode p_1. (b) The eigenmode pressure in the vertical yz microchannel cross-section at $x = 0$. (c) The eigenmode pressure in the horizontal xy plane at channel mid-height $z = 0$. Reproduced with changes from Ref. [184] with permission.

To model the system, the liquid-filled microchannel is treated as a liquid-filled rectangular cuboid whose boundary conditions represent the surrounding chip. Here, We assume that the walls confining the liquid inside the chancel are acoustically infinitely hard compared to the liquid. When considering a silicon microchannel containing water, the difference between the acoustic impedance of water (denser and more compressible than silicon) $Z_{\mathrm{wa}} = \rho_{\mathrm{wa}} c_{\mathrm{wa}} = 1.5\,\mathrm{MPas/m}$ and the wall $Z_{\mathrm{si}} = \rho_{\mathrm{si}} c_{\mathrm{si}} = 20\,\mathrm{MPas/m}$ causes $\sim 75\%$ of the incident acoustic energy to be reflected on each impact. The reflection coefficient (R) is defined as

$$R = \left(\frac{Z_{\mathrm{si}} - Z_{\mathrm{wa}}}{Z_{\mathrm{si}} + Z_{\mathrm{wa}}} \right)^2 \approx 75\%, \tag{3.1}$$

Such a value for R suggests that the simplifications mentioned earlier are reasonable. However, it is not unexpected if the acoustic field in the bulk outside the channel, to some extent, also impacts the resonance mode inside the channel.

The acoustic cavity in the model has a length l, width w, and height h. To find the eigenfrequencies and later the time-harmonic ultrasound pressure field $p_1 \exp(-i\omega t)$ where $\omega = 2\pi f$ is the angular velocity and f the driving frequency, the so-called lossy Helmholtz wave equation [187] needs to be solved for a hard wall boundary condition.

$$4\nabla^2 p_1 = -k^2 p_1, \quad \text{BC: } \boldsymbol{n} \cdot \boldsymbol{\nabla} p_1 = 0, \tag{3.2}$$

where $k = \omega / c_{\mathrm{m}}$ is the wavevector, $\boldsymbol{n}$ is an outward pointing vector orthogonal to the walls, and c_{m} is the speed of sound in the liquid. The viscous damping coefficient is discarded in this version of the Helmholtz wave equation since it is around 10^{-6} for 2-MHz ultrasound oscillations in water at 25°C.
Solving the Eq. (3.2) results in the following eigenfrequencies

$$f_{n_x,n_y,n_z} = \frac{c_{\mathrm{m}}}{2} \sqrt{\frac{n_x^2}{l^2} + \frac{n_y^2}{w^2} + \frac{n_z^2}{h^2}} \quad \text{with } n_x, n_y, n_z = 0, 1, 2, 3, ..., \tag{3.3}$$

n_x, n_y, n_z are the number of half-wavelengths along x, y, z, respectively. The corresponding eigenfunction p_1 becomes

$$p_1(x, y, z) = p_{\mathrm{a}} \cos\left(k_x (x + \frac{L}{2}) \right) \cos\left(k_y (y + \frac{w}{2}) \right) \cos\left(k_z (z + \frac{h}{2}) \right), \tag{3.4}$$

where p_{a} is the pressure amplitude, and $k_j = n_j \frac{\pi}{L_j}$ is the wavenumber along each spatial direction. Based on Eq. (3.3), if the resonant frequency is close to

$f = c_\mathrm{m}/\lambda = c_\mathrm{m}/(2w)$, the number of periods along the length of the channel is minimal. This can be seen in Fig. 3.2, where We plot the (20, 1, 0)-mode for a section of the microchannel with 2 mm length around the center $x = 0$. Throughout this thesis, We assume $n_x < 20$, and in our case, within a microscope field of view, the eigenfunction p_1 reduces to a nearly transversal mode as described by the plan wave Eq. (3.5). Additionally, in systems with continuous flow, the variations along x cancel according to their periodic nature.

$$p_1 = p_\mathrm{a} \cos\left(k_y(y + \frac{w}{2})\right). \tag{3.5}$$

The energy carried by acoustic waves is a combination of the kinetic energy of the moving fluid elements and the potential energy of the compressed fluid, which is necessary for the acoustic manipulation of particles/cells. By inserting Eq. (3.5) in the general expression of the total time-averaged acoustic energy density (see further details in Ref. [188]), We get the 1D acoustic energy density (E_ac) for the purely transverse mode

$$E_\mathrm{ac} = \frac{p_\mathrm{a}^2}{4\rho_\mathrm{m} c_\mathrm{m}^2} = \frac{1}{4}\kappa_\mathrm{m} p_\mathrm{a}^2 = \frac{1}{4}\rho_\mathrm{m} v_\mathrm{a}^2 \tag{3.6}$$

where ρ_m is the fluid density, $\kappa_\mathrm{m} = 1/(\rho_\mathrm{m} c_\mathrm{m}^2)$ compressibility, and v_a is the amplitude of the oscillation velocity.

3.3 Acoustic Radiation Force

The widely referenced theory for the acoustic radiation force acting on a compressible particle suspended in an inviscid fluid was initially formulated by Gorkov [189]. Grokov in 1962 summarized and generalized the works of King [190], Yosioka, and Kawasima [191]. He builds up his theory based on the assumption that "the magnitude of the force is equal to the average flux of momentum through any closed surface in the fluid which encloses the particle." [189] When subjected to a sound wave (the wavelength is here assumed to be much larger than the size of the sphere), the sphere scatters and thereby interferes locally with the pressure field. As a result, the sphere becomes compressed by the acoustic pressure field and oscillates in response to the acoustic velocity field. Lately, building upon the approach of Gorkov, Settnes and Bruus extended the theoretical expression of the acoustic radiation force acting on a compressible, spherical, and small particle to include the viscosity of the suspending fluid [192]. The reader is referred to Refs. [193]–[195] for more information on the analysis and mathematical treatment.

A single monopole and a single dipole term can describe the scattering. The monopole presents a compressible and stationery particle that causes scattering due to the compressibility difference between the particle and the surrounding

fluid. The dipole term considers a moving incompressible particle resulting in scattering due to the density difference between the particle and surrounding fluid. The acoustic radiation force arises due to the differences in acoustic properties between a particle (subscript p) of radius a and the surrounding viscous fluid (subscript m). The time-averaged acoustic radiation force on a suspended single small spherical particle is given by [192]

$$\boldsymbol{F}_{\mathrm{rad}} = -\pi a^3 \left\{ \frac{2\kappa_{\mathrm{m}}}{3} \mathrm{Re}\left[f_1 p_1 \boldsymbol{\nabla} p_1\right] - \rho_{\mathrm{m}} \mathrm{Re}\left[f_2 \boldsymbol{v}_1 \cdot \boldsymbol{\nabla} \boldsymbol{v}_1\right] \right\}, \tag{3.7}$$

where f_1 and f_2 are given by

$$f_1(\tilde{\kappa}) = 1 - \tilde{\kappa}, \quad \text{with } \tilde{\kappa} = \frac{\kappa_{\mathrm{p}}}{\kappa_{\mathrm{m}}}, \tag{3.8a}$$

$$f_2\left(\tilde{\rho}, \tilde{\delta}\right) = \frac{2\left[1 - \Gamma\left(\tilde{\delta}\right)\right](\tilde{\rho} - 1)}{2\tilde{\rho} + 1 - 3\Gamma\left(\tilde{\delta}\right)}, \quad \text{with } \tilde{\rho} = \frac{\rho_{\mathrm{p}}}{\rho_{\mathrm{m}}}, \tag{3.8b}$$

$$\tilde{\Gamma}\left(\tilde{\delta}\right) = -\frac{3}{2}\left[1 + \mathrm{i}\left(1 + \tilde{\delta}\right)\right]\tilde{\delta}, \quad \text{with } \tilde{\delta} = \frac{\delta}{a}. \tag{3.8c}$$

f_1 denotes the contribution from the pressure field and f_2 from the velocity field to the acoustic radiation force ($\boldsymbol{F}_{\mathrm{rad}}$) on the particle. In Eq. (3.8), Γ is the viscous correction factor to $\boldsymbol{F}_{\mathrm{rad}}$ and δ viscous boundary layer thickness. In the particular scenario of the horizontal transverse pressure resonance described in Eq. (3.5), the expression of the resulting radiation force simplifies to [191]

$$\boldsymbol{F}_{\mathrm{rad}} = 4\pi a^3 \Phi\left(\tilde{\kappa}, \tilde{\rho}, \tilde{\delta}\right) k_y E_{\mathrm{ac}} \sin\left(2k_y(y + \frac{w}{2})\right), \tag{3.9}$$

where

$$\Phi\left(\tilde{\kappa}, \tilde{\rho}, \tilde{\delta}\right) = \frac{1}{3} f_1(\tilde{\kappa}) + \frac{1}{2} \mathrm{Re}\left[f_2\left(\tilde{\rho}, \tilde{\delta}\right)\right], \tag{3.10}$$

is the so-called acoustic contrast factor. In the acoustic radiation force $\boldsymbol{F}_{\mathrm{rad}}$ formula, Eq. (3.9), the factor $\sin\left(2k_y(y + \frac{w}{2})\right)$ determines the maxima and minima. Note that the compressibility and density of particles/cells relative to the suspending medium in Φ dictate the sign and magnitude of the force. For positive contrast factors ($\Phi > 0$), the force is oriented towards the pressure nodes of the standing wave (channel center), while for negative ($\Phi < 0$), it is directed towards the anti-nodes (channel walls) [Fig. 3.3]. Throughout the work of this thesis, the contrast factor plays an important role. In Paper I, We tune the contrast factor of cells by altering the density and compressibility of the suspending medium and study the three-dimensional trajectories of cells. The rest of the Papers are based on isoacoustic focusing, where We characterize and separate cells when their contrast factor becomes zero.

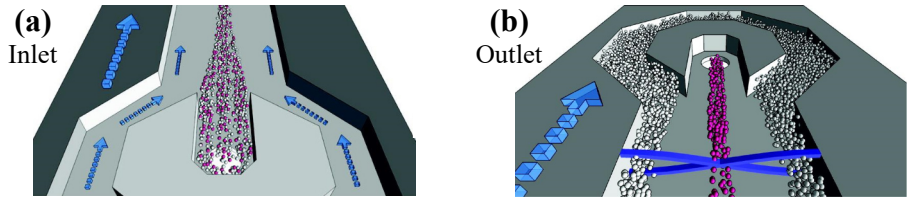

Figure 3.3: Illustration of acoustophoretic separation of proteins (pink) from fatty lipids (white) within a continuous system (arrows). This method is applied in the sample preparation for the analysis of raw milk. (a) Initially, at the intent, the mixture of proteins and lipids occupies the central stream in the channel. (b) At the outlet, the lipids ($\Phi < 0$) move to the pressure anti-nodes at the sidewalls, while the small proteins ($\Phi > 0$) remain in the central region. Adapted with permission from Grenvall *et al.* [196].

3.4 Boundary-induced Acoustic Streaming

In 1884, Lord Rayleigh published his well-known analysis of the boundary-driven acoustic streaming velocity $\langle \boldsymbol{v}_2 \rangle$ in an infinite parallel plate channel of height h hosting a first-order bulk velocity field with a horizontal y-component of the form $v_{1y} = v_\mathrm{a} \sin\left(k_y(y + \frac{w}{2})\right)$ corresponding to the first-order pressure p_1 given in Eq. (3.5) and illustrated in Fig. 3.2(b). In the case of an isothermal fluid and with the assumption $\lambda \gg h \gg \delta$, Rayleigh found time-averaged components $\langle v_{2y} \rangle$ and $\langle v_{2z} \rangle$ of the streaming velocity $\langle \boldsymbol{v}_2 \rangle$ outside the viscous boundary layer to be [197]

$$\langle v_{2y} \rangle = \frac{3}{16} \frac{v_\mathrm{a}^2}{c_\mathrm{m}} \sin(2k_y(y + \frac{w}{2})) \left[1 - 3\frac{z^2}{(h/2)^2}\right], \tag{3.11a}$$

$$\langle v_{2z} \rangle = \frac{3}{16} \frac{v_\mathrm{a}^2}{c_\mathrm{m}} k_y h \cos(2k_y(y + \frac{w}{2})) \left[\frac{z^3}{(h/2)^3} - \frac{z}{h/2}\right]. \tag{3.11b}$$

Figure 3.4 shows the resulting $\langle \boldsymbol{v}_2 \rangle$ in the microchannel cross-section for the transverse half-wave resonance in Eq. (3.5) and Fig. 3.2(b). At the plates $z = \pm h/2$, the z-component $\langle v_{2z} \rangle$ of the $\langle \boldsymbol{v}_2 \rangle$ becomes zero, and the often-cited streaming velocity u_str just outside the viscous boundary layer appears to be

$$\langle v_{2y}^\mathrm{bnd} \rangle = u_\mathrm{str} = -\frac{3}{8} \frac{v_\mathrm{a}^2}{c_\mathrm{m}} \sin(2k_y(y + \frac{w}{2})) = -\frac{3}{2} \frac{E_\mathrm{ac}}{\rho_\mathrm{m} c_\mathrm{m}} \sin(2k_y(y + \frac{w}{2})). \tag{3.12}$$

By inserting $z = 0$ for the channel mid-height, $\langle v_{2z} \rangle$ vanishes and the expression

of the velocity along y becomes

$$\langle v_{2y}^{\mathrm{mid}} \rangle = \frac{3}{16} \frac{v_{\mathrm{a}}^2}{c_{\mathrm{m}}} \sin(2k_y(y + \frac{w}{2})). \tag{3.13}$$

Throughout the work of this thesis, E_{ac} is determined using three-dimensional trajectories (next section) of 1.1-μm-diameter polystyrene (PS) particles with known density and compressibility. In brief, the velocity of the tracks around the mid-height ($z = 0$), where both acoustic radiation and streaming follow a sinusoidal dependency on y, were fitted to a function $u_y = u_0 \sin(2k_y y + \alpha)$ where u_0 and α are free fitting parameters. For more details, the reader is referred to the section determination of the acoustic energy density in Papers I [198] and II [199].

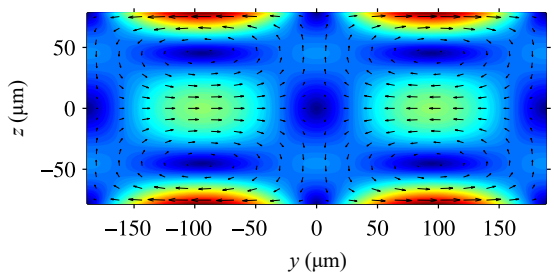

Figure 3.4: Vector plot (black arrows) of the acoustic streaming $\langle \boldsymbol{v}_2 \rangle$ and color plot of its magnitude $\langle v_2 \rangle$ from zero (dark blue) to maximum (dark red). Note that the plots based on Rayleigh's result in Eq. (3.11b) are valid for an isothermal liquid sandwiched between two parallel plates of height h and the assumption $\lambda \gg h \gg \delta$. The streaming is induced by a standing ultrasound pressure wave as in Eq. (3.5) with wavelength $\lambda_y = 2\pi/k_y$ or $k_y = \pi/w$ for $n_y = 1$. Adapted with changes from Ref. [200] with permission.

3.5 Acoustophoretic Trajectories

The physics of time-averaged acoustophoretic particle/cell trajectories is crucial to understanding acoustofluidic-based separation. The acoustophoretic trajectories in homogeneous fluid in microchannels result from the nonlinear time-averaged acoustic radiation force and the streaming-induced drag and have been studied experimentally using particle tracking, microparticle image velocimetry, and optical traps, as well as numerical investigations.

3.5.1 The Equation of Motion

For a single spherical particle/cell of radius a and mass m_p suspended in a fluid perturbed by an acoustic field of wavelength $\lambda \gg a$, the equation of motion for particles/cells as a point particle/cell with velocity $\boldsymbol{v}_\mathrm{p}$ based on Newton's second law becomes [185]

$$m_\mathrm{p}\frac{d\boldsymbol{v}_\mathrm{p}}{dt} = \boldsymbol{F}_\mathrm{rad} + \boldsymbol{F}_\mathrm{drag} + \boldsymbol{F}_\mathrm{buoy}. \tag{3.14}$$

The single-particle theory may be valid for dilute suspensions, but when dealing with more concentrated solutions (above $\sim 1\%$ particle-volume-concentration), the effects of particle-particle interactions are expected to become notably pronounced [201]. The calculation of the acoustic radiation force $\boldsymbol{F}_\mathrm{rad}$ on the particle/cells is based on Eq. (3.7), which holds true for any incident acoustic field (p_1 and $\boldsymbol{v}_1$) in the long-wavelength limit $a \ll \lambda$ [192].
In small Reynolds numbers, the viscous drag force $\boldsymbol{F}_\mathrm{drag}$ is given by

$$\boldsymbol{F}_\mathrm{drag} = 6\pi\eta_\mathrm{m}a(\boldsymbol{v} - \boldsymbol{v}_\mathrm{p}). \tag{3.15}$$

Here, $\boldsymbol{v}$ is the fluid velocity. When We disregard the particle-induced streaming, this velocity is essentially the same as the external boundary-driven streaming velocity. It is worth noting that particles/cells moving close to the channel walls face an increased drag force, as indicated in previous studies [200]. However, this specific contribution is not considered in this thesis. Finally, the combined force of buoyancy and gravity $\boldsymbol{F}_\mathrm{buoy}$ by incorporating the gravitational acceleration $\boldsymbol{g}$ and the term $\tilde{\rho} = \rho_\mathrm{p}/\rho_\mathrm{m}$ is equivalent to

$$\boldsymbol{F}_\mathrm{buoy} = \frac{4}{3}\pi a^3(\tilde{\rho} - 1)\rho_\mathrm{m}\boldsymbol{g}. \tag{3.16}$$

In the microfluidics context, neglecting the inertial acceleration term found in the equation of motion Eq. (3.14) is often valid. This is because the inertia-to-acoustic force ratio (β) becomes very small. To exemplify, for a 50 μm polystyrene particle and $E_\mathrm{ac} = 100\ \mathrm{J/m^3}$, $\beta = 8k_y^2a^4(\rho_\mathrm{p}-\rho_\mathrm{m})E_\mathrm{ac}\Phi/(81\pi\eta_\mathrm{m}^2)) \approx 0.001$ (see further details in Refs. [185], [202]). By neglecting inertia, Eq. (3.14) directly provides the particle/cell velocity,

$$\boldsymbol{v}_\mathrm{p} = \frac{1}{6\pi\eta_\mathrm{m}a}(\boldsymbol{F}_\mathrm{rad} + \boldsymbol{F}_\mathrm{buoy}) + \boldsymbol{v}. \tag{3.17}$$

Typically, in acoustofluidic experiments with microparticles/cells, the radiation force and/or the drag force due to streaming dominate the particle/cell motion; however, in cases with altered suspending media, the buoyancy force contributes to the final shape of the trajectories as well which was one of the main findings in Paper I.

3.5.2 Critical Particle Size

Large qualitative differences emerge when comparing particle trajectories dominated by the radiation force $\boldsymbol{F}_{\mathrm{rad}}$ and those governed by the drag force $\boldsymbol{F}_{\mathrm{drag}}$ induced by acoustic streaming. As illustrated in Fig. 3.5, the radiation force nails particles to a location of zero force (nodes in the case of polystyrene (PS) beads due to their positive contrast), while the streaming continuously propels particles in a swirling motion.

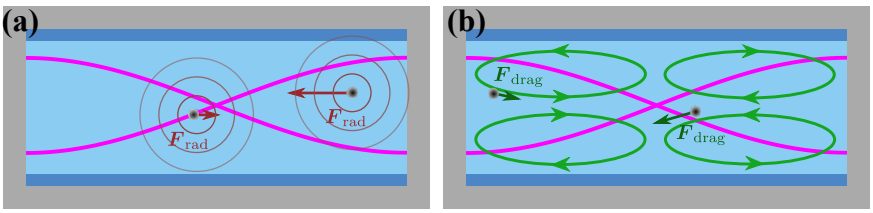

Figure 3.5: Schematic of the typical PS particle trajectories in the cross-section of a channel filled with homogeneous fluid and exposed to a standing half-wave acoustic field across the width (magenta). (a) Due to the scattering of the sound field around the particles (surrounding circles), the acoustic radiation force ($\boldsymbol{F}_{\mathrm{rad}}$) displaces the particles to eh center of the channel. (b) For the particles smaller than the critical size, streaming-induced drag force ($\boldsymbol{F}_{\mathrm{drag}}$) maintains the particles along the streaming rolls (green loops). Continuous swirling motion is caused by the boundary layer (dark blue). Adapted from Ref. [203].

The ratio of the magnitudes of these two forces is often calculated at the mid-plane to determine whether a particle's trajectory is predominantly influenced by radiation or streaming. The magnitude of $\boldsymbol{F}_{\mathrm{rad}}$ is derived from Eq. (3.9), while the magnitude of $\boldsymbol{F}_{\mathrm{drag}}$ acting on a stationary particle ($v_{\mathrm{p}} = 0$) is determined using Eq. (3.15) with the fluid velocity amplitude equal to the Rayleigh streaming amplitude of Eq. (3.12) expressed by means of the acoustic energy density E_{ac}. Both forces scale with E_{ac}; therefore, this term cancels out in the ratio and yields

$$\frac{|\boldsymbol{F}_{\mathrm{rad}}|}{|\boldsymbol{F}_{\mathrm{drag}}|} = \frac{4}{9}\frac{\Phi a^2 \rho_{\mathrm{m}} \omega}{\eta_{\mathrm{m}}}, \tag{3.18}$$

where now the scaling becomes quadratic with particle size, leading to the conclusion that the trajectories of large particles are primarily governed by radiation force, while the trajectories of small particles are streaming-dominated [200], [204]. The transition between these two regimes of motion occurs at a critical particle size (a_{crit}), obtained by equating the force ratio in Eq. (3.18),

$$a_{\mathrm{crit}} \approx \sqrt{\frac{9}{4}\frac{\eta_{\mathrm{m}}}{\Phi\rho_{\mathrm{m}}\omega}} \approx 1\,\mu\mathrm{m}, \tag{3.19}$$

where the resulting value is calculated based on the experimental model system for a PS particle suspended in water at 2 MHz. As a result, in acoustophoresis, a common practice is to distinguish between large particles ($2a \gtrsim 5\,\mu$m), such as cells, and submicron nanoparticles ($2a \lesssim 1\,\mu$m), such as bacteria, and vesicles [205].

3.5.3 Trajectories of Suspension Cells

Cells suspended in standard media, such as PBS, behave similarly to large PS particles, and their trajectories are radiation-dominated due to the positive contrast factor ($\Phi > 0$). However, in a media of altered density and compressibility (by adding iodixanol to PBS), cells can acquire negative ($\Phi < 0$) and zero ($\Phi \approx 0$) contrast factors. In a sense, tuning the acoustic properties of the suspending media to change the cell's contrast factor is the foundation of iso-acoustic focusing. When $\Phi < 0$, the acoustic radiation force is still in charge of the motion but in the opposite direction moving the cells towards the pressure antinodes (channel side walls). In the last scenario ($\Phi \approx 0$), cells are acoustically transparent, and the acoustic radiation force becomes negligible; thus, cells follow the typical streaming rolls in the cross-section in response to the streaming-induced drag force. Based on the Eqs. (3.8) and (3.10), density and compressibility of the cells relative to the suspending media determine the contrast factor value, that is, there should be a combination that yields zero for the summation of $\frac{1}{3}f_1$ and $\frac{1}{2}f_2$.

Paper I extensively examines the three-dimensional trajectories of various cell types suspended in homogeneous media for different contrast factors. This Paper extends the application of defocused image-based tracking to suspension cells. The tracking method, in the first step, takes defocused microscope images of particles at different depth positions of the channel and stores them in a look-up table (reference library). Finally, the algorithm maps the z-component of the trajectory for each particle by cross-correlation with the reference images (see further details in Paper I). For an acoustic cavity filled with an inhomogeneous medium (next chapter), the acoustic streaming is substantially suppressed; therefore, acoustic radiation force drives the cells according to their local contrast factor. Paper II investigates the trajectories of cells based on defocused-shape tracking in gradients of acoustic impedances.

3.6 Refined Acoustophoresis

Microchannel acoustophoresis has been widely demonstrated for a variety of applications. Amongst others, this technique has been used to focus, wash, concentrate, separate, sort, and trap particles/cells.[206]–[212] While flowing through an acoustic half-wave resonator, cells are pushed sideways and gathered in the pressure nodes along the center plane, and when reaching the far end of such a resonator, the cells can be collected in different outlet fractions by splitting up the flow, Fig. 3.6(a-c).

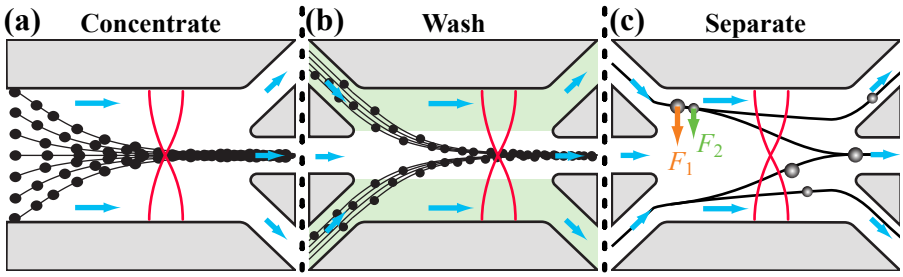

Figure 3.6: Overview schematics of acoustic separation modalities. Schematics are reproduced with permission from Per Augustsson.

Cell separation by acoustic radiation forces works based on the underlying biophysical properties density, compressibility, and mainly cell size. The separation is contact-free and exerts forces on cells comparable in magnitude to centrifugation with the clear benefit of being straightforwardly implemented for in-line processing [168]. However, the conventional acoustophoresis struggles with three main limitations. The method is highly size-dependent, and such dependency has hampered the development of cell analyzers based on the underlying properties of cell density and compressibility. This shortcoming also is shared by most microfluidic techniques relying on size and volume-based forces. It should be noted that the size of cells can vary a factor of 2 within a given cell type with large overlaps between sub-groups of a population. Although examples exist of canceling the size dependency via balancing against gravity [213], loading cells with immuno-affinity microbeads [214], [215], no conventional acoustophoretic method exists that allows for size-independent cell separation. Acoustophoretic cell separation works for dilute cell suspensions and faces challenges when processing whole blood as input which is the starting point of many tests [201], [216]. The difficulty is due to the fact that WBCs become dragged along with the highly abundant RBCs as they migrate to the central node of a separation channel. Lastly, due to the acoustic streaming, the acoustophoretic separation of nanoparticles is quite challenging [204], [217].

Isoacoustic focusing (IAF) is a refined version of the acoustophoretic method, which analyses cells based on their acoustic properties and enables size-insensitive separation. Acoustic characterization of tissue is highly valuable in medicine, particularly in various medical ultrasound imaging applications such as sound scattering, attenuation, and elasticity.[218], [219] Sound velocity and attenuation have been successfully mapped at a sub-cellular level for adherent cells through acoustic microscopy, suggesting a connection between acoustic properties and the internal content and structure of a cell [220]–[223]. Although measurements using standard density and sound velocity meters can provide information about the average acoustic properties of cell populations in suspension [224], the acoustic properties of individual suspension cells are not fully charted. IAF measures single cells' effective acoustic impedance, which is a function of density and compressibility and provides an opportunity to decouple them from one another [199], [225]. Density and compressibility are the keys to fully determining the transport of a cell in an acoustic resonator filled with any medium; however, the acoustofluidics community has not been able to resolve it yet. Within the field, there are several studies that investigated cells' migration in acoustic fields to measure cell compressibility [226]–[232]. The cells' so-called acoustophoretic mobility is then measured, and by assuming the density of a specific cell type to be the same as the population average from literature, the compressibility of single cells is calculated.

Drawbacks with these methods are that (i) cells' densities, and sometimes radii, are inserted based on previously reported values and are not measured in the experiments, thereby introducing uncertainties in estimating the measured quantities, (ii) it is assumed that the property of a single cell can be represented by the population average, and (iii) reference particles, normally made from polystyrene can vary considerably in their acoustic properties despite being made from the same material [233]. Paper IV addresses this pitfall and proposes an upgraded version of IAF to determine the compressibility by an independent measurement of the density.

Furthermore, in IAF, cells can be processed at high concentrations because the stabilizing acoustic body force present in the medium prevents inter-particle hydrodynamic coupling [201]. Finally, Due to the thousand-fold suppression of acoustic streaming in the presence of inhomogeneity [234], [235], IAF pushes the lower size limit to the sub-micrometer regime. The next chapter provides a summary of experimental IAF.

Chapter 4

Isoacoustic Focusing

Looking into the biophysical properties of cells at the single-cell level is a promising tool for cell classification that involves evaluating key parameters associated with differences or changes in the interior structure of a cell. This approach aims to demonstrate that a cell's biophysical signature can provide insight into its phenotype as well as changes in cell state and disease progress. Within the acoustofluidics community, introducing IAF was the first attempt to analyze the effective acoustic impedance of single cells (Z_c) in continuous flow and, more importantly, in a size-insensitive manner [225]. A schematic illustration of the principle of IAF is shown in Fig. 4.1. As cells flow through a microchannel, they undergo lateral displacement due to the influence of the acoustic radiation force from a transverse pressure resonance p_1, toward streams of increasing acoustic impedance in an inhomogeneous medium. The cells continue the sideways migration until they reach their cell-type-specific isoacoustic point IAP) where $\Phi \approx 0$ for $Z_c = Z_m$. The acoustic radiation force diminishes at this point, and the sideways displacement ceases. Cell-specific differences in the effective acoustic impedance Z_c result in a spatial dispersion of the cell population over the channel cross-section and allow continuous label-free analysis and separation of individual cells. Here, the method can be seen as a microfluidic equivalent of density-gradient centrifugation, where the control parameter acoustic impedance $Z = \sqrt{\rho/\kappa}$ is replaced for the density ρ. The technique operates based on tailoring a smooth acoustic impedance gradient employing an acoustically stabilized iodixanol concentration gradient and the ability to address the cell positions in the gradient optically. IAF, in its first appearance, was used to measure the effective acoustic impedance of thousands of individual cells, including monocytes, lymphocytes, neutrophils, BA-F3, and MCF7 cells, in just a few minutes [225]. The technique was later adapted to separate cancer cells from white blood cells [236] and bacterial manipulation [217].

The work of this thesis stands on the shoulder of IAF and investigates var-

ious details regarding the method. In Paper II, We show how cells reach their IAP in a stop-flow format of IAF and discuss the requirements for measuring their effective acoustic impedance. In Paper III, We introduce the acoustic impedance gradient in the presence of undiluted blood to separate PBMCs from RBCs. Finally, in Paper IV, We upgrade the IAF read-out platform with a density gradient centrifugation module to address the density and compressibility of cells. This chapter provides a brief description of the different aspects of the IAF setup.

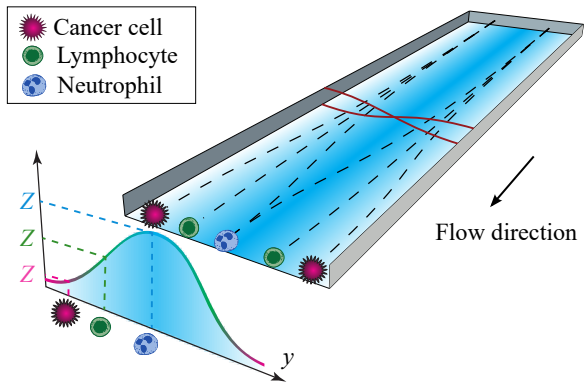

Figure 4.1: Illustration of isoacoustic focusing for size-insensitive characterization of individual cells, such as cancer cells and white blood cells. In the experiments, cells are carried through a channel while an acoustic pressure field directs them sideways into media of gradually increasing or decreasing acoustic impedance Z (blue shading, Gaussian curve). As cells approach the end of the channel, their sideways position depends on their phenotype-specific acoustic impedance, since it is focused in the position for which $Z_c = Z_m$. Schematic is reproduced with permission from Per Augutsson.

4.1 The Acoustic Body Force

The work of IAF originates from a set of experiments with fluids that uncovered that inhomogeneities in density and compressibility, introduced by a solute concentration field, can be acoustically relocated into stabilized configurations. Deshmukh *et al.* [237] showed in 2014 that for two media of different acoustic impedances, laminated next to each other, the medium with higher acoustic impedance moves toward the pressure node. They demonstrated that even a tiny difference as low as 0.1% in the acoustic impedance of the two media leads to fluid relocation and stabilizing the interface between them against gravity. Later, Karlsen [185], during his Ph.D., studied the underlying physics of this

phenomenon and expressed the acoustic body force. For more detail on the mathematical expression of the acoustic body force acting on inhomogeneous fluids, the reader is referred to Refs. [185], [238]. The acoustic body force has been studied for different applications, such as stabilization of concentration gradients against gravitational collapse (see Fig. 4.2) [238], suppression of acoustic streaming [234], [235], and patterning concentration fields [239].

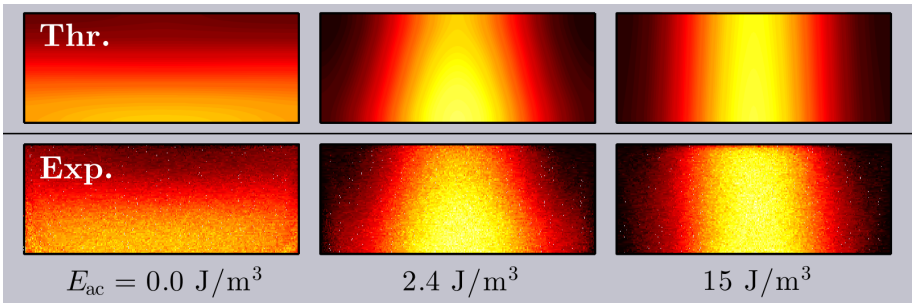

Figure 4.2: Simulation (top) and experimental (bottom) outcome of creation and maintenance of a concentration gradient in an acoustofluidic channel with a half-wave acoustic resonance for three different acoustic energies $E_{ac} = 0$, 2.4, and 15 J/m^3. Figure adapted with permission from Ref. [238].

4.2 Acoustic Streaming Suppression

Rayleigh streaming is a key limiting factor in the context of standing wave acoustic manipulation of microparticles. Suspended microparticles in this regime are subjected to acoustic radiation force and Stokes drag force resulting from the acoustic streaming. As described in the previous chapter, the microparticle size and the material properties of the particle and the surrounding medium determine the relative magnitude of these two forces. For particles smaller than the critical size, acoustic streaming dominates the motion and, in many cases, hinders the manipulation of submicrometer-sized particles in homogenous media. However, in the case of inhomogeneous media, it was recently found that the acoustic body force arising from the spatial inhomogeneity in density and compressibility efficiently suppresses the acoustic streaming in the bulk inside a half-wavelength resonator. Figure 4.3 shows the experimental trajectories of 1.1 μm in diameter PS particles in homogeneous (a and c) and inhomogeneous media (b) 30 seconds after the actuation of sound. Numerical and experimental studies by Karlesen *et al.* [234] and Qiu *et al.* [235], [240] focus on acoustic streaming in inhomogeneous fluids, where solute concentration gradients introduce density and compressibility variations. They show that (i) the com-

petition between boundary-induced streaming and the inhomogeneity-induced acoustic force density introduces a dynamic length scale for the streaming vortex size, (ii) initially, this dynamic length scale is much smaller than the vortex size observed in homogeneous fluids, and (iii) as time progresses, diffusion and advection cause the dynamic length scale to increase, eventually leading to streaming patterns similar to those in homogeneous fluids.

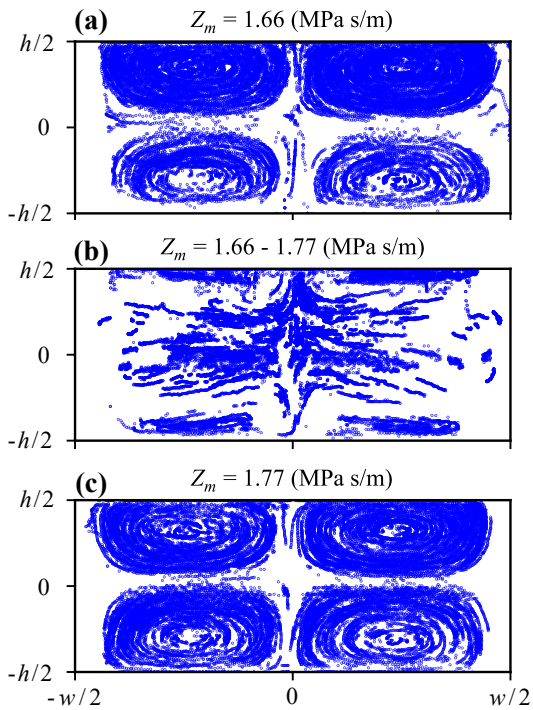

Figure 4.3: Experimental trajectories of 1.1 μm in diameter PS particles in (a) homogenous medium of $Z_m = 1.66$ MPa s/m, (b) a gradient from $Z_m = 1.66$ to 1.77 MPa s/m, and (c) homogenous medium of $Z_m = 1.77$ MPa s/m.

4.3 Cells at the Isoacoustic Point

The acoustic contrast factor for cells, given by Eq. (4.1), at their IAP is zero. In general, the IAP of a cell depends on four parameters: ρ_c, κ_c, ρ_m, and κ_m,

$$\Phi = \frac{1-\tilde{\kappa}}{3} + \frac{\tilde{\rho}-1}{2\tilde{\rho}+1}, \tag{4.1}$$

where $\tilde{\kappa} = \kappa_c/\kappa_m$ and $\tilde{\rho} = \rho_c/\rho_m$ are the relative compressibility and density of the cell with respect to the suspending medium. In this thesis, based on Ref. [225], the acoustic impedance ($Z = \sqrt{\rho/\kappa}$) has been used to quantify the IAP when there is no access to all these parameters. Ref. [225] shows that in the IAP, the effective acoustic impedance of cells (Z_c) is approximately equal to that of the local iodixanol concentration field (Z_m) within 0.8% of all combination for ρ_c (range of 1000 kg/m^3 to 1200 kg/m^3) and κ_c (range of 3.4×10^{-10} Pa^{-1} to 4.4×10^{-10} Pa^{-1}). For further details on the relative impedance difference between the medium and the cells at the IAP, the reader is referred to Ref. [225]. In Paper IV, since we have access to ρ_c, ρ_m, and κ_m, we can determine the compressibility of cells (κ_c) residing in their IAP by

$$\Phi = 0 \longleftrightarrow \kappa_c = \kappa_m \left(\frac{5\tilde{\rho} - 2}{2\tilde{\rho} + 1} \right). \tag{4.2}$$

4.4 Experimental Considerations

The experimental acoustophoresis system in the IAF read-out platform and mainly in Paper IV includes a prefocusing unit [Fig. 4.4]. Different factors impact the magnitude of the acoustic radiation force and the outcome of the particle/cell manipulation using ultrasonic standing wave fields. The following sections outline some of the common practical considerations when designing an acoustic experiment.

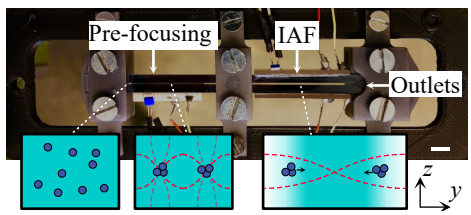

Figure 4.4: Acoustofluidic chip with a schematic of the cross-sectional view of the pre-alignment channel where cells (blue) are aligned by a standing wave field (dashed red curves) and the IAF channel where an acoustic resonant pressure field locates pre-focused cells into their IAP.

Acoustophoretic Pre-alignment

After being introduced to the acoustofluidic chip, cells are randomly distributed in the cross-section of the channel. Therefore, they experience different flow velocities due to the parabolic flow profile. Cells located near the top, bottom, and side walls of the channel move at a very low flow speed and thus spend

more time in the acoustic standing wave field compared to cells positioned farther away from the surrounding structures. This scenario can reduce the efficiency and purity of the cell separation. This challenge has been addressed by introducing a pre-alignment step prior to acoustic separation, particularly for particles/cells of different sizes [241]. In the pre-alignment unit, the acoustic field is designed to have two pressure nodes in the horizontal plane and one pressure node in the vertical plane (see pre-focusing in Fig. 4.4). While passing through, particles/cells are aligned both in width and height, and they enter the next channel with the same starting position and flow velocity. Consequently, the separation relies solely on the acoustic properties of particles/cells and is not biased by the starting position. The significance of pre-alignment has been demonstrated across various applications [242], [243]. In Paper IV, We investigate its impact while measuring the effective acoustic impedance of cells. One advantage of the pre-alignment step for IAF experiments is that cells are already elevated to a certain height, and that provides better control for imaging at the end of the channel.

Side Actuation

The magnitude of the acoustic radiation force determines the throughput for certain separation tasks, and it depends on several factors, including particle volume, acoustic contrast factor, frequency, and acoustic energy density. In biomedical applications, bioparticles typically need to be carried in media with good biocompatibility, resulting in low acoustic contrast factors and lower acoustic radiation force. Increasing frequency can increase this force [244], but for a resonant cavity operating at its fundamental resonance mode, such an increase results in a decrease in the cavity size, reducing the sample volumes that can be processed. Consequently, increasing the acoustic energy density within the microchannel, which scales linearly with the acoustic radiation force, is crucial to improving the acoustophoresis device throughput [245]–[247]. Traditionally, one way to increase the acoustic energy density is to applying high electric power to piezoelectric transducers using power amplifiers. However, this leads to energy loss, temperature rise, and potential harm to biological samples. In bulk acoustophoresis devices, typically, the piezoelectric transducer has been attached to the bottom of the chip. This so-called bottom actuation offers ease of transducer mounting and a larger coupling area but requires high electrical power to achieve a sufficient acoustic energy density [248], [249]. Recently, Qiu *et al.* [170] investigated an alternative way to actuate the system, namely, in the same direction as the standing-wave field by gluing the transducer to the side of the chip. They demonstrated that the energy density and acoustic radiation force in acoustophoresis devices may be increased by a factor of 4 using side actuation, improving the energy conversion efficiency. In this thesis, side actuation was implemented in Papers II and IV.

Temperature

Bulk acoustic wave devices are prone to heat generation in higher applied voltages due to the actuation of the piezoceramic transducers (PZT) and energy losses within the PZT material; therefore, it is important to monitor the temperature since it can affect the performance of the acoustofluidic device. It has been revealed that acoustic resonance peak shifts by approximately 1 kHz for every degree Celsius change in temperature [250]. A temperature change of 5°C can entirely alter the resonance mode of the device. Additionally, in the work of this thesis, the gradient field is extracted based on the intensity profile of a fluorescent dye. Hence, the change in temperature can alter the intensity profile and result in inaccurate measurement of the acoustic impedance. In all the included Papers, the temperature was kept at ∼22°C, and in the case of temperature increase, the device was cooled down by airflow.

Chapter 5

Summary of the Included Papers

The work of this thesis investigates isoacoustic focusing to characterize and separate suspension cells. Although the included Papers in a broad perspective serve a shared goal, each Paper addresses a specific objective. Papers I and II deal with the physics of acoustophoretic trajectories of suspension cells in homogenous and inhomogeneous media. Paper III makes use of the built knowledge to separate target cells from undiluted blood by altering the acoustic properties of the plasma. Finally, Paper IV describes an upgraded version of isoacoustic focusing platform to report the density and compressibility of cells. This chapter communicates a brief summary of the main result for each included Paper and considers two questions to be answered: (i) What motivated the study? and (ii) what are the main results?

5.1 Paper I: Acoustofluidic Three-Dimensional Motion of Suspended Cells at Near-Zero Acoustic Contrast in Homogeneous Media

Paper I focuses on understanding cell motion in homogeneous suspending media of different acoustic impedances exposed to an acoustic half-standing wave. The primary goal was to investigate the role of acoustic streaming and buoyancy, particularly for suspension cells with near-zero acoustic contrast. When the acoustic contrast is close to zero, the radiation force becomes negligible, and cells primarily follow the acoustic streaming flow. This study fills this gap by investigating the three-dimensional motion of suspended cells due to acoustic radiation force, acoustic streaming, and buoyancy inside an acoustofluidic

resonator. Three-dimensional trajectories were measured using the defocusing-based particle tracking method, and the results were compared to numerical modeling [Fig. 5.1]. Paper I shows that neutrally buoyant cells have a positive contact factor, and acoustic streaming in homogeneous media limits the separation of cells of similar but non-overlapping acoustic properties.

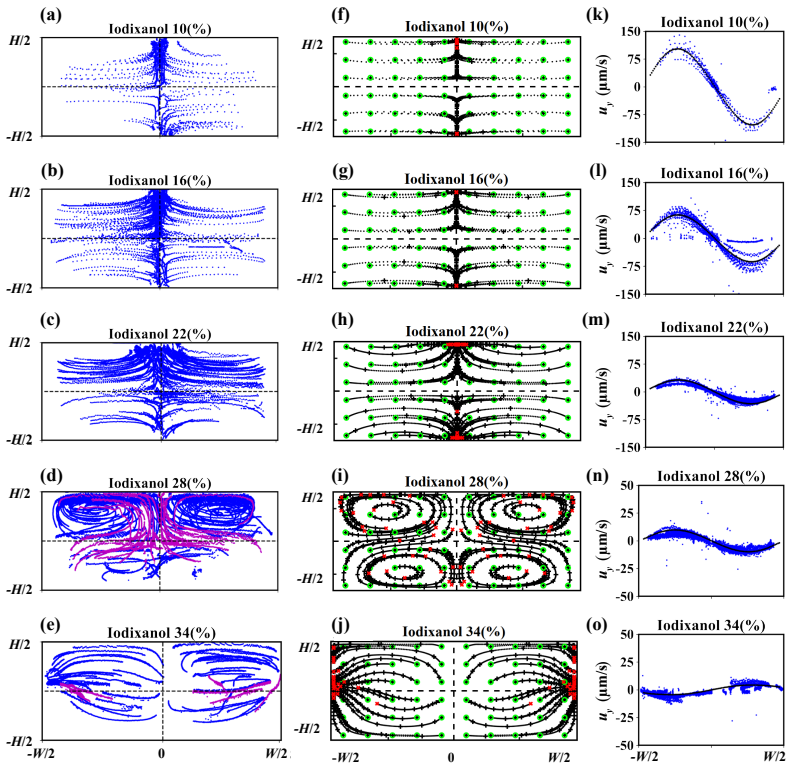

Figure 5.1: Three-dimensional trajectories of neutrophils in different concentrations of iodixanol projected along x. (a)–(c) The contrast factor is positive for neutrophils, and they end up in the center of the channel within 10 s of recording after the onset of the sound. (d) In the scenario where the acoustic impedance of the medium matches that of the neutrophils, the acoustic radiation force vanishes. Recording time was 30 s. (e) Trajectories of neutrophils of negative contrast factor forcing them towards the walls. Recording time was 20 s. (a)–(e) Cells that transition from the lower to the upper half are indicated in magenta. (f)–(j) Simulated trajectories of neutrophils for the same range of iodixanol concentrations as in (a)–(e). The initial and final locations of neutrophils in the simulations are marked with green circles and red crosses, respectively. (k)–(o) Experimental (blue dots) and simulated (black dots) data for y-component of neutrophil velocity at mid-height. The time step is 0.1 s for all measured and simulated trajectories.

5.2 Paper II: Acoustophoretic Characterization and Separation of Blood Cells in Acoustic Impedance Gradients

Paper II investigates cell motion in a stopped-flow format of isoacoustic focusing to understand the factors influencing individual cells while traveling towards their IAP. Parameters such as cell radius, density, compressibility, acoustic energy density, and gradient in material properties in the fluid are examined. This study employs a numerical model to simulate the trajectories of cells in diffusing iodixanol gradients based on measured gradients and their evolution over time and compare it to experimental trajectories [Fig. 5.2]. This study estimated the acoustic energy density in the layered configuration of fluids by fitting the model to measured data of PS beads. Paper II demonstrates that the streaming-free environment enabled by the acoustic impedance gradients makes this approach beneficial compared to the separation of cells in a homogeneous medium of tailored acoustic impedance.

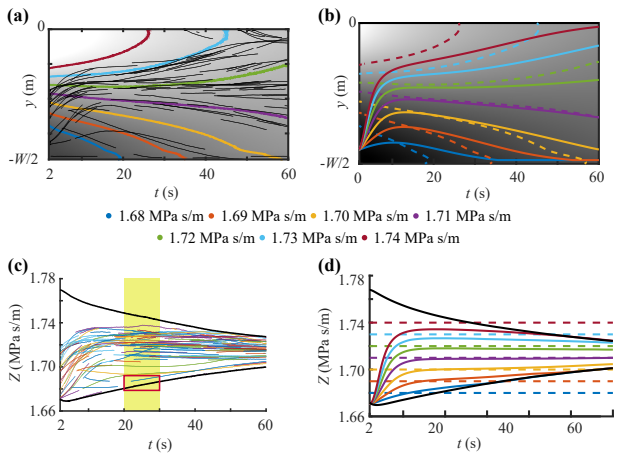

Figure 5.2: Experimental and simulated cell trajectories. (a) Neutrophil y-coordinate vs. time in an acoustic impedance gradient (black curves). Z_m is indicated by grayscale values spanning from 1.64 MPa s/m (black) to 1.75 MPa s/m (white). Colored contours indicate constant Z_m. (b) Plot of simulated trajectories $y_c(t)$ for cells of hypothetical Z_c (thick colored lines) in the same acoustic impedance gradient as in (a). Z_m is indicated by grayscale values spanning from 1.68 MPa s/m (black) to 1.74 MPa s/m (white). (c) Experimentally measured the effective acoustic impedance of neutrophils vs. time when assigning $Z_c = Z_m$. (multiple cells can have the same color). Solid black lines indicate Z_m at the channel walls (lower line) and center (upper line). The yellow region shows the time span of the measurement, and the red box highlights a cell with properties outside the measurable range. (d) Simulated Z_m (solid lines) and true Z_c (dashed lines) for hypothetical cells.

5.3 Paper III: Label-Free Separation of Peripheral Blood Mononuclear Cells from Whole Blood by Gradient Acoustic Focusing

Paper III deals with the separation of peripheral blood mononuclear cells (PBMCs) from whole blood, which is a crucial step in various medical and research applications. The study relies on the microchannel acoustophoresis and tunes the acoustic properties of the suspending medium and the blood plasma to enrich PBMCs from RBCs and granulocytes. Two flow-through separation approaches, one using a barrier medium and the other altering the acoustic properties of the blood plasma, were used to achieve efficient PBMC separation from undiluted or minimally diluted blood samples. In Paper III, We enriched PBMCs relative to RBCs by a factor of 3600 to 11000 and with a separation efficiency of 85% [Fig. 5.3]. Such a level of RBC depletion is high compared to most other microfluidic methods and similar to density centrifugation output. The designed chip in this study runs up to 20 µl/min undiluted whole blood and can be easily integrated with downstream analysis.

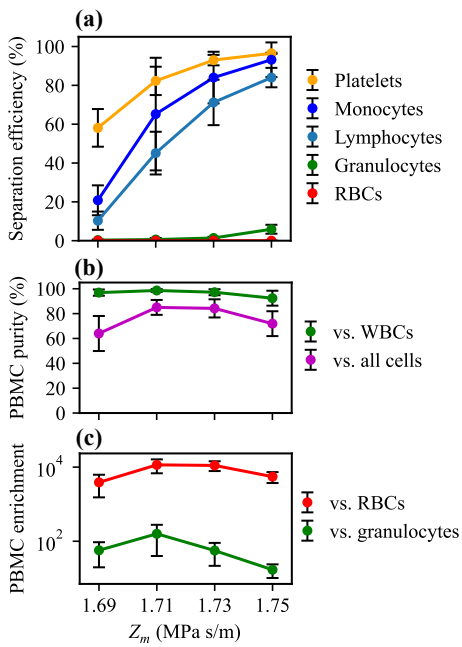

Figure 5.3: Barrier medium separation. (a) Separation efficiency, (b) output purity, and (c) relative enrichment of PBMCs compared to other cells (log scale). Data points are average values of $n = 5$ experiments with $\pm$ one standard deviation.

5.4 Paper IV: Microfluidic Compressibility Cytometry Using Isoacoustic Focusing Integrated with Density Centrifugation

Paper IV addresses the importance of measuring the density and compressibility of cells in predicting and optimizing acoustophoretic cell separation and classification. In acoustofluidics research field, there are several studies on compressibility cytometry; however, those studies include drawbacks such as assuming cells' density based on previously reported values and a property of a single cell can be represented by the population average. At this cell-specific isoacoustic point, compressibility can be determined by an independent measurement of the density of each cell. This study pre-sorts neutrophils and K562 cells off-chip in linear, continuous, and reproducible density gradients and feeds four density fractions with a known density as an input into an isoacoustic focusing chip. Paper IV investigates the relation between density and compressibility for two cell types and finds for K562 cells negative correlation, with compressibility decreasing from $3.77 \pm 0.04 \times 10^{-10}$ Pa^{-1} to $3.71 \pm 0.04 \times 10^{-10}$ Pa^{-1} for increasing density. For neutrophils, the compressibility of $3.675 \pm 0.035 \times 10^{-10}$ Pa^{-1} was measured, which was unchanged for increasing density [Fig. 5.4].

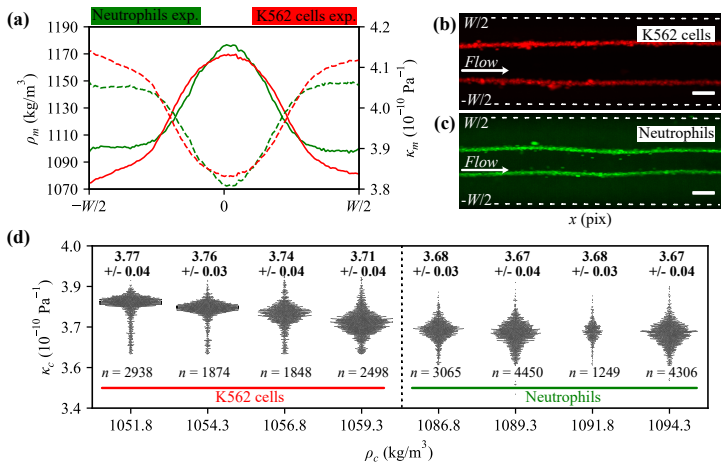

Figure 5.4: Compressibility cytometry of neutrally buoyant cells. (a) Profile of medium density (solid line) and compressibility (dashed line) extracted from the fluorescent dextran images for experiments with neutrophils (green, for $\rho_c = 1089.3$ kg/m^3) and K562 cells (red, for $\rho_c = 1059.3$ kg/m^3). (b) and (c) Cell image overlay of 100 images are shown for (b) K562 cells and (c) neutrophils. (d) Distribution of cell compressibility for cells of different densities. The scale bar in (b) and (c) is 100 μm.

Chapter 6

Conclusions and Outlook

In many biological and clinical assays, an efficient cell separation routine as a preparatory step is required. Such a need has resulted in the recent development of various microscale separation technologies that exploit cell's unique biophysical signatures to classify them in a label-free format. These technologies, compared to macroscale cell handling techniques, offer high precision and flexibility for single-cell phenotyping, require small sample volumes, and include external forces in the microscale to deterministically position cells in the microchannel. The work of this thesis demonstrates the use of acoustophoretic forces to characterize and separate suspension cells. Microchannel acoustophoresis is an established gentle and contact-free technique for particle and cell manipulation, and the driving acoustic radiation force is comparable in magnitude to that of centrifugation, with the clear benefit of being straightforwardly implemented for in-line processing. However, the size-dependent nature of the technique has not allowed the development of cell analysis modules to infer the underlying biophysical properties of the cells (density and compressibility). In this thesis, a refined version of the acoustophorresis method called isoacoustic focusing is explored to overcome size dependency for cell separation and to measure the density and compressibility of single cells. The first two studies presented herein provide a better understanding of the acoustophoretic trajectories of cells in both homogeneous and inhomogeneous media and highlight the effect of acoustic streaming regarding the separation outcome. To further optimize acoustic cell separations, these studies emphasize the importance of accurate knowledge about the size, density, and compressibility at the single-cell level, which is currently missing in the literature. Acoustic focusing combined with altered acoustic properties of plasma in Paper III was proven applicable for the enrichment of peripheral mononuclear cells from undiluted blood and achieved comparable throughput in terms of whole blood equivalent volume flow per processing channel to inertial focusing with a better separation

performance while using undiluted blood as a direct input. Moreover, the isoacoustic read-out platform in Paper IV was upgraded with a density gradient centrifugation unit to enable high-throughput compressibility cytometry.

Much effort was invested throughout the work of this thesis to characterize suspension cells by isoacoustic focusing; however, additional work and time is needed to address all the challenges associated with the current platform. The setup, as it is described in Paper IV, aims to do cell cytometry by extracting the biophysical properties of cells. To further validate the method, it would be useful to fabricate test particles of known density, compressibility, and size similar to cells and monitor their isoacoustic point. Such standard density marker beads can be used to calibrate the density gradient and the acoustic field. To include the size and shape of the cells when they arrive at their isoacoustic point, fast bright field imaging can be implemented. Throughout the work of this thesis, the gradient profile was extracted via the iodixanol concentration field based on the assumption that iodixanol molecules and dextran fluorescent dye diffuse approximately in the same way. For future studies, to avoid this assumption, it is suggested to implement optical approaches to read out the iodixanol concentration in the isoacoustic focusing channel, for instance, by reporting the refractive index of the medium. In this thesis, to perform multicolor fluorescence imaging, cells were stained with dyes that are designed to freely pass through cell membranes into cells and are nontoxic at working concentrations. Further research needs to be done to provide more information on how staining can possibly alter the biophysical properties of cells. Changes in cell density naturally occur on different occasions, such as cell cycle, metabolic status (e.g., activation and starvation), differentiation, and pathological conditions (e.g., apoptosis and sickle cell disease). For future studies, it would be interesting to monitor some of these changes using the setup introduced in Paper IV.

References

[1] *How microdevices revolutionize deep space exploration*, https://microtas-2023.org/program/speakers.html.

[2] H. Bruus, *Theoretical Microfluidics*. Oxford University Press, 2007.

[3] Y. Wang, W.-Y. Lin, K. Liu, *et al.*, "An integrated microfluidic device for large-scale in situ click chemistry screening," *Lab Chip*, vol. 9, pp. 2281–2285, 16 2009.

[4] G. M. Whitesides, "The origins and the future of microfluidics," *Nature 2006 442:7101*, vol. 442, no. 7101, pp. 368–373, Jul. 2006.

[5] G. M. Whitesides and A. D. Stroock, "Flexible Methods for Microfluidics," *Physics Today*, vol. 54, no. 6, pp. 42–48, Jun. 2001.

[6] Y. Song, Y.-Y. Huang, X. Liu, X. Zhang, M. Ferrari, and L. Qin, "Point-of-care technologies for molecular diagnostics using a drop of blood," *Trends in Biotechnology*, vol. 32, no. 3, pp. 132–139, 2014.

[7] D. Wu and J. Voldman, "An integrated and automated electronic system for point-of-care protein testing," in *2019 41st Annual International Conference of the IEEE Engineering in Medicine and Biology Society (EMBC)*, 2019, pp. 1571–1574.

[8] J. D. Caplin, N. G. Granados, M. R. James, R. Montazami, and N. Hashemi, "Microfluidic organ-on-a-chip technology for advancement of drug development and toxicology," *Advanced Healthcare Materials*, vol. 4, no. 10, pp. 1426–1450, 2015.

[9] P. M. Mafla-Endara, V. Meklesh, J. P. Beech, P. Ohlsson, M. Pucetaite, and E. C. Hammer, "Exposure to polystyrene nanoplastics reduces bacterial and fungal biomass in microfabricated soil models," *Science of The Total Environment*, vol. 904, p. 166 503, 2023.

[10] H. W. Hou, A. A. S. Bhagat, W. C. Lee, S. Huang, J. Han, and C. T. Lim, "Microfluidic Devices for Blood Fractionation," *Micromachines 2011, Vol. 2, Pages 319-343*, vol. 2, no. 3, pp. 319–343, Jul. 2011.

[11] J. F. Dailey, *Dailey's Notes on blood*. Medical Consulting Group, 2002.

[12] K. D. Pagana and T. J. Pagana, *Mosby's Diagnostic and Laboratory Test Reference - eBook*. Elsevier Health Sciences, 2010.

[13] P. Sethu, A. Sin, and M. Toner, "Microfluidic diffusive filter for apheresis (leukapheresis)," *Lab Chip*, vol. 6, pp. 83–89, 2006.

[14] "Medical gallery of blausen medical," *WikiJournal of Medicine*, vol. 1, 2014.

[15] S. V. Rudmann, *Textbook of Blood Banking and Transfusion Medicine*. Elsevier Health Sciences, 2005.

[16] G. J. Tortora and B. Derrickson, *Principles of Anatomy and Physiology*. Wiley, 2014.

[17] A. Jemal, F. Bray, M. M. Center, J. Ferlay, E. Ward, and D. Forman, "Global cancer statistics," *CA: A Cancer Journal for Clinicians*, vol. 61, no. 2, pp. 69–90, 2011.

[18] H. Esmaeilsabzali, T. V. Beischlag, M. E. Cox, A. M. Parameswaran, and E. J. Park, "Detection and isolation of circulating tumor cells: Principles and methods," *Biotechnology Advances*, vol. 31, no. 7, pp. 1063–1084, 2013, Stem Cell Engineering.

[19] G. P. Gupta and J. Massagué, "Cancer metastasis: Building a framework," *Cell*, vol. 127, no. 4, pp. 679–695, 2006.

[20] A. van de Stolpe, K. Pantel, S. Sleijfer, L. W. Terstappen, and J. M. den Toonder, "Circulating tumor cell isolation and diagnostics: Toward routine clinical use," *Cancer Research*, vol. 71, no. 18, pp. 5955–5960, Sep. 2011.

[21] T. Ashworth, "A case of cancer in which cells similar to those in the tumours were seen in the blood after death," *Aust Med J.*, vol. 14, p. 146, 1869.

[22] C. Wittekind and M. Neid, "Cancer invasion and metastasis," *Oncology*, vol. 69, no. Suppl. 1, pp. 14–16, Oct. 2005.

[23] E. Racila, D. Euhus, A. J. Weiss, *et al.*, "Detection and characterization of carcinoma cells in the blood," *Proceedings of the National Academy of Sciences*, vol. 95, no. 8, pp. 4589–4594, 1998.

[24] V. A. Adalsteinsson and J. C. Love, "Toward engineered processes for sequencing-based analysis of single circulating tumor cells," *Current Opinion in Chemical Engineering*, vol. 4, pp. 97–104, 2014.

[25] L. Descamps, D. L. Roy, and A. L. Deman, "Microfluidic-Based Technologies for CTC Isolation: A Review of 10 Years of Intense Efforts towards Liquid Biopsy," *International Journal of Molecular Sciences 2022, Vol. 23, Page 1981*, vol. 23, no. 4, p. 1981, Feb. 2022.

[26] *Enumerating ctc in humans*, www.vycap.com/application/circula-ting-tumor-cells/.

[27] M. T. Gabriel, L. R. Calleja, A. Chalopin, B. Ory, and D. Heymann, "Circulating Tumor Cells: A Review of Non–EpCAM-Based Approaches for Cell Enrichment and Isolation," *Clinical Chemistry*, vol. 62, no. 4, pp. 571–581, Apr. 2016.

[28] E. Ozkumur, A. M. Shah, J. C. Ciciliano, *et al.*, "Inertial focusing for tumor antigen-dependent and -independent sorting of rare circulating tumor cells," *Science Translational Medicine*, vol. 5, no. 179, Apr. 2013.

[29] *Cancer cell line encyclopedia*, https://sites.broadinstitute.org/ccle/.

[30] J. Carrot-Zhang, X. Yao, S. Devarakonda, *et al.*, "Whole-genome characterization of lung adenocarcinomas lacking alterations in the rtk/ras/raf pathway," *Cell Reports*, vol. 34, no. 5, p. 108 707, 2021.

[31] Y. Zheng, J. Nguyen, Y. Wei, and Y. Sun, "Recent advances in microfluidic techniques for single-cell biophysical characterization," *Lab on a Chip*, vol. 13, no. 13, pp. 2464–2483, Jun. 2013.

[32] Y. Zhao, K. Wang, D. Chen, *et al.*, "Development of microfluidic impedance cytometry enabling the quantification of specific membrane capacitance and cytoplasm conductivity from 100,000 single cells," *Biosensors and Bioelectronics*, vol. 111, pp. 138–143, Jul. 2018.

[33] D. Spencer and H. Morgan, "High-Speed Single-Cell Dielectric Spectroscopy," *ACS Sensors*, vol. 5, no. 2, pp. 423–430, Feb. 2020.

[34] Y. Feng, L. Huang, P. Zhao, F. Liang, and W. Wang, "A Microfluidic Device Integrating Impedance Flow Cytometry and Electric Impedance Spectroscopy for High-Efficiency Single-Cell Electrical Property Measurement," *Analytical Chemistry*, vol. 91, no. 23, pp. 15 204–15 212, Dec. 2019.

[35] S. Stavrakis, G. Holzner, J. Choo, and A. deMello, "High-throughput microfluidic imaging flow cytometry," *Current Opinion in Biotechnology*, vol. 55, pp. 36–43, Feb. 2019.

[36] G. Holzner, B. Mateescu, D. van Leeuwen, *et al.*, "High-throughput multiparametric imaging flow cytometry: toward diffraction-limited sub-cellular detection and monitoring of sub-cellular processes," *Cell Reports*, vol. 34, no. 10, p. 108 824, Mar. 2021.

[37] A. A. Nawaz, M. Urbanska, M. Herbig, *et al.*, "Intelligent image-based deformation-assisted cell sorting with molecular specificity," *Nature Methods 2020 17:6*, vol. 17, no. 6, pp. 595–599, May 2020.

[38] M. Lippeveld, C. Knill, E. Ladlow, *et al.*, "Classification of Human White Blood Cells Using Machine Learning for Stain-Free Imaging Flow Cytometry," *Cytometry Part A*, vol. 97, no. 3, pp. 308–319, Mar. 2020.

[39] P. Eulenberg, N. Köhler, T. Blasi, *et al.*, "Reconstructing cell cycle and disease progression using deep learning," *Nature Communications 2017 8:1*, vol. 8, no. 1, pp. 1–6, Sep. 2017.

[40] K. C. Lee, J. Guck, K. Goda, and K. K. Tsia, "Toward Deep Biophysical Cytometry: Prospects and Challenges," *Trends in Biotechnology*, vol. 39, no. 12, pp. 1249–1262, Dec. 2021.

[41] Y. Chen, Z. Zhou, S. Zhu, Z. Ni, and N. Xiang, "Label-free microfluidics for single-cell analysis," *Microchemical Journal*, vol. 177, p. 107 284, Jun. 2022.

[42] K. Kaladharan, A. Kumar, P. Gupta, K. Illath, T. S. Santra, and F. G. Tseng, "Microfluidic Based Physical Approaches towards Single-Cell Intracellular Delivery and Analysis," *Micromachines 2021, Vol. 12, Page 631*, vol. 12, no. 6, p. 631, May 2021.

[43] T. Zangle and M. Teitell, "Live-cell mass profiling: An emerging approach in quantitative biophysics," *Nature Methods*, vol. 11, pp. 1221–1228, 2014.

[44] Y. K. Park, C. Depeursinge, and G. Popescu, "Quantitative phase imaging in biomedicine," *Nature Photonics 2018 12:10*, vol. 12, no. 10, pp. 578–589, Sep. 2018.

[45] R. J. Kimmerling, S. M. Prakadan, A. J. Gupta, *et al.*, "Linking single-cell measurements of mass, growth rate, and gene expression 06 biological sciences 0604 genetics," *Genome Biology*, vol. 19, no. 1, pp. 1–13, Nov. 2018.

[46] L. Mu, J. H. Kang, S. Olcum, *et al.*, "Mass measurements during lymphocytic leukemia cell polyploidization decouple cell cycle- And cell size-dependent growth," *Proceedings of the National Academy of Sciences of the United States of America*, vol. 117, no. 27, pp. 15 659–15 665, Jul. 2020.

[47] N. Cermak, S. Olcum, F. F. Delgado, *et al.*, "High-throughput measurement of single-cell growth rates using serial microfluidic mass sensor arrays," *Nature Biotechnology 2016 34:10*, vol. 34, no. 10, pp. 1052–1059, Sep. 2016.

[48] A. Zipursky, E. Bow, R. S. Seshadri, and E. J. Brown, "Leukocyte density and volume in normal subjects and in patients with acute lymphoblastic leukemia," *Blood*, vol. 48, no. 3, pp. 361–371, Sep. 1976.

[49] M. Delarue, G. P. Brittingham, S. Pfeffer, *et al.*, "mTORC1 Controls Phase Separation and the Biophysical Properties of the Cytoplasm by Tuning Crowding," *Cell*, vol. 174, no. 2, pp. 338–349, Jul. 2018.

[50] W. Choi, C. Fang-Yen, K. Badizadegan, *et al.*, "Tomographic phase microscopy," *Nature Methods 2007 4:9*, vol. 4, no. 9, pp. 717–719, Aug. 2007.

[51] M. Urbanska, H. E. Muñoz, J. Shaw Bagnall, *et al.*, "A comparison of microfluidic methods for high-throughput cell deformability measurements," *Nature Methods 2020 17:6*, vol. 17, no. 6, pp. 587–593, Apr. 2020.

[52] E. M. Darling and D. Di Carlo, "High-Throughput Assessment of Cellular Mechanical Properties," *Annual Review of Analytical Chemistry*, vol. 17, pp. 35–62, Dec. 2015.

[53] P. Rosendahl, K. Plak, A. Jacobi, *et al.*, "Real-time fluorescence and deformability cytometry," *Nature Methods 2018 15:5*, vol. 15, no. 5, pp. 355–358, Apr. 2018.

[54] D. R. Gossett, H. T. Tse, S. A. Lee, *et al.*, "Hydrodynamic stretching of single cells for large population mechanical phenotyping," *Proceedings of the National Academy of Sciences of the United States of America*, vol. 109, no. 20, pp. 7630–7635, May 2012.

[55] B. Fregin, F. Czerwinski, D. Biedenweg, *et al.*, "High-throughput single-cell rheology in complex samples by dynamic real-time deformability cytometry," *Nature Communications 2019 10:1*, vol. 10, no. 1, pp. 1–11, Jan. 2019.

[56] O. Otto, P. Rosendahl, A. Mietke, *et al.*, "Real-time deformability cytometry: on-the-fly cell mechanical phenotyping," *Nature Methods 2015 12:3*, vol. 12, no. 3, pp. 199–202, Feb. 2015.

[57] K. D. Nyberg, K. H. Hu, S. H. Kleinman, D. B. Khismatullin, M. J. Butte, and A. C. Rowat, "Quantitative Deformability Cytometry: Rapid, Calibrated Measurements of Cell Mechanical Properties," *Biophysical Journal*, vol. 113, no. 7, pp. 1574–1584, Oct. 2017.

[58] J. R. Lange, J. Steinwachs, T. Kolb, *et al.*, "Microconstriction Arrays for High-Throughput Quantitative Measurements of Cell Mechanical Properties," *Biophysical Journal*, vol. 109, no. 1, pp. 26–34, Jul. 2015.

[59] C. Macaraniag, Q. Luan, J. Zhou, and I. Papautsky, "Microfluidic techniques for isolation, formation, and characterization of circulating tumor cells and clusters," *APL Bioengineering*, vol. 6, no. 3, p. 31 501, Sep. 2022.

[60] S. W. Choe, B. Kim, and M. Kim, "Progress of Microfluidic Continuous Separation Techniques for Micro-/Nanoscale Bioparticles," *Biosensors 2021, Vol. 11, Page 464*, vol. 11, no. 11, p. 464, Nov. 2021.

[61] B. A. Kidd, G. Hoffman, N. Zimmerman, *et al.*, "Evaluation of direct-to-consumer low-volume lab tests in healthy adults," *The Journal of Clinical Investigation*, vol. 126, no. 5, pp. 1734–1744, May 2016.

[62] A. Urbansky, *Acoustofluidic preparation of whole blood components*. Ph.D. thesis, Lund University, 2019.

[63] F. Olm, *Label-free processing of stem cell preparations by acoustophoresis*. Ph.D. thesis, Lund University, 2020.

[64] M. Antfolk, *Acoustofluidic rare cell sample preparation*. Ph.D. thesis, Lund University, 2015.

[65] R. G. Miller and R. A. Phillips, "Separation of cells by velocity sedimentation," *Journal of Cellular Physiology*, vol. 73, no. 3, pp. 191–201, Jun. 1969.

[66] *Guide to the Preparation, Use and Quality Assurance of Blood Components: Recommendation No. R (95) 15*. Council of Europe, 2007.

[67] P. R. Amable, R. B. V. Carias, M. V. T. Teixeira, *et al.*, "Platelet-rich plasma preparation for regenerative medicine: Optimization and quantification of cytokines and growth factors," *Stem Cell Research and Therapy*, vol. 4, no. 3, pp. 1–13, Jun. 2013.

[68] M. K. Beakke, "Density Gradient Centrifugation: A New Separation Technique," *Journal of the American Chemical Society*, vol. 73, no. 4, pp. 1847–1848, Apr. 1951.

[69] T. B. Casale and M. Kaliner, "A rapid method for isolation of human mononuclear cells free of significant platelet contamination," *Journal of Immunological Methods*, vol. 55, no. 3, pp. 347–353, Dec. 1982.

[70] H. Pertoft, T. C. Laurent, T. Låås, and L. Kågedal, "Density gradients prepared from colloidal silica particles coated by polyvinylpyrrolidone (Percoll)," *Analytical Biochemistry*, vol. 88, no. 1, pp. 271–282, Jul. 1978.

[71] H. Hakonarson, U. S. Bjornsdottir, E. Halapi, *et al.*, "Profiling of genes expressed in peripheral blood mononuclear cells predicts glucocorticoid sensitivity in asthma patients," *Proceedings of the National Academy of Sciences of the United States of America*, vol. 102, no. 41, pp. 14 789–14 794, Oct. 2005.

[72] K. Kovacovicova and M. Vinciguerra, "Isolation of senescent cells by iodixanol (OptiPrep) density gradient-based separation," *Cell Proliferation*, vol. 52, no. 6, e12674, Nov. 2019.

[73] F. Brosseron, K. Marcus, and C. May, "Isolating peripheral lymphocytes by density gradient centrifugation and magnetic cell sorting," *Methods in Molecular Biology*, vol. 1295, pp. 33–42, 2015.

[74] C. Pösel, K. Möller, W. Fröhlich, I. Schulz, J. Boltze, and D. C. Wagner, "Density Gradient Centrifugation Compromises Bone Marrow Mononuclear Cell Yield," *PLOS ONE*, vol. 7, no. 12, e50293, Dec. 2012.

[75] N. Y. Naung, S. Suttapreyasri, S. Kamolmatyakul, and T. Nuntanaranont, "Comparative study of different centrifugation protocols for a density gradient separation media in isolation of osteoprogenitors from bone marrow aspirate," *Journal of Oral Biology and Craniofacial Research*, vol. 4, no. 3, pp. 160–168, Sep. 2014.

[76] S. Miltenyi, W. Müller, W. Weichel, and A. Radbruch, "High gradient magnetic cell separation with MACS," *Cytometry*, vol. 11, no. 2, pp. 231–238, Jan. 1990.

[77] H. Abts, M. Emmerich, S. Miltenyi, A. Radbruch, and H. Tesch, "CD20 positive human B lymphocytes separated with the magnetic cell sorter (MACS) can be induced to proliferation and antibody secretion in vitro," *Journal of Immunological Methods*, vol. 125, no. 1-2, pp. 19–28, Dec. 1989.

[78] D. K. Moore, B. Motaung, N. du Plessis, A. N. Shabangu, A. G. Loxton, and C. Su-Irg, "Isolation of B-cells using Miltenyi MACS bead isolation kits," *PLOS ONE*, vol. 14, no. 3, e0213832, Mar. 2019.

[79] Y. C. Eun, C. J. Kyeong, J. P. Hyo, *et al.*, "Thymocyte-thymocyte interaction for efficient positive selection and maturation of CD4 T cells," *Immunity*, vol. 23, no. 4, pp. 387–396, Oct. 2005.

[80] R. Weiss, W. Gerdes, F. Leonhardt, R. Berthold, U. Sack, and A. Grahnert, "A comparative study of two separation methods to isolate monocytes," *Cytometry Part A*, vol. 95, no. 2, pp. 234–241, Feb. 2019.

[81] T. Lozar, T. Jesenko, V. Kloboves Prevodnik, *et al.*, "Preclinical and Clinical Evaluation of Magnetic-Activated Cell Separation Technology for CTC Isolation in Breast Cancer," *Frontiers in Oncology*, vol. 10, p. 554 554, Sep. 2020.

[82] J. F. Edd, A. Mishra, K. C. Smith, *et al.*, "Isolation of circulating tumor cells," *iScience*, vol. 25, no. 8, p. 104 696, Aug. 2022.

[83] J. H. Dykes, J. Toporski, G. Juliusson, *et al.*, "Rapid and effective CD3 T-cell depletion with a magnetic cell sorting program to produce peripheral blood progenitor cell products for haploidentical transplantation in children and adults," *Transfusion*, vol. 47, no. 11, pp. 2134–2142, Nov. 2007.

[84] A. Grützkau and A. Radbruch, "Small but mighty: How the MACS®-technology based on nanosized superparamagnetic particles has helped to analyze the immune system within the last 20 years," *Cytometry Part A*, vol. 77A, no. 7, pp. 643–647, Jul. 2010.

[85] B. D. Plouffe, S. K. Murthy, and L. H. Lewis, "Fundamentals and application of magnetic particles in cell isolation and enrichment: a review," *Reports on Progress in Physics*, vol. 78, no. 1, p. 016 601, Dec. 2014.

[86] S. S. Leong, S. P. Yeap, and J. K. Lim, "Working principle and application of magnetic separation for biomedical diagnostic at high- and low-field gradients," *Interface Focus*, vol. 6, no. 6, Dec. 2016.

[87] W. A. Bonner, H. R. Hulett, R. G. Sweet, and L. A. Herzenberg, "Fluorescence Activated Cell Sorting," *Review of Scientific Instruments*, vol. 43, no. 3, pp. 404–409, Mar. 1972.

[88] D. Galbraith, "Flow cytometry and cell sorting: The next generation," *Methods*, vol. 57, no. 3, pp. 249–250, Jul. 2012.

[89] S. F. Ibrahim and G. Van Den Engh, "Flow cytometry and cell sorting," *Advances in Biochemical Engineering/Biotechnology*, vol. 106, pp. 19–39, Jun. 2007.

[90] D. R. Gossett, W. M. Weaver, A. J. MacH, *et al.*, "Label-free cell separation and sorting in microfluidic systems," *Analytical and Bioanalytical Chemistry*, vol. 397, no. 8, pp. 3249–3267, Aug. 2010.

[91] F. Shiri, H. Feng, and B. K. Gale, "Passive and active microfluidic separation methods," *Particle Separation Techniques: Fundamentals, Instrumentation, and Selected Applications*, pp. 449–484, Jan. 2022.

[92] P. J. Kenis, R. F. Ismagilov, and G. M. Whitesides, "Microfabrication inside capillaries using multiphase laminar flow patterning," *Science*, vol. 285, no. 5424, pp. 83–85, Jul. 1999, see https://felicefrankel.com/covers/.

[93] H. M. Ji, V. Samper, Y. Chen, C. K. Heng, T. M. Lim, and L. Yobas, "Silicon-based microfilters for whole blood cell separation," *Biomedical Microdevices*, vol. 10, no. 2, pp. 251–257, Apr. 2008.

[94] S. Zheng, H. K. Lin, B. Lu, *et al.*, "3D microfilter device for viable circulating tumor cell (CTC) enrichment from blood," *Biomedical Microdevices*, vol. 13, no. 1, pp. 203–213, Feb. 2011.

[95] H. Mohamed, J. N. Turner, and M. Caggana, "Biochip for separating fetal cells from maternal circulation," *Journal of Chromatography A*, vol. 1162, no. 2, pp. 187–192, Aug. 2007.

[96] Y. Cheng, X. Ye, Z. Ma, S. Xie, and W. Wang, "High-throughput and clogging-free microfluidic filtration platform for on-chip cell separation from undiluted whole blood," *Biomicrofluidics*, vol. 10, no. 1, Jan. 2016.

[97] X. Li, W. Chen, G. Liu, W. Lu, and J. Fu, "Continuous-flow microfluidic blood cell sorting for unprocessed whole blood using surface-micromachined microfiltration membranes," *Lab on a Chip*, vol. 14, no. 14, pp. 2565–2575, Jun. 2014.

[98] M. Zinggeler, T. Brandstetter, and J. Rühe, "Biophysical Insights on the Enrichment of Cancer Cells from Whole Blood by (Affinity) Filtration," *Scientific Reports 2019 9:1*, vol. 9, no. 1, pp. 1–11, Feb. 2019.

[99] P. Chen, X. Feng, W. Du, and B. F. Liu, "Microfluidic chips for cell sorting," *Frontiers in Bioscience*, vol. 13, no. 7, pp. 2464–2483, Jan. 2008.

[100] S. Goto, Y. Ikeda, E. Saldívar, and Z. M. Ruggeri, "Distinct mechanisms of platelet aggregation as a consequence of different shearing flow conditions," *The Journal of Clinical Investigation*, vol. 101, no. 2, pp. 479–486, Jan. 1998.

[101] S. Nomura, N. N. Tandon, T. Nakamura, J. Cone, S. Fukuhara, and J. Kambayashi, "High-shear-stress-induced activation of platelets and microparticles enhances expression of cell adhesion molecules in thp-1 and endothelial cells," *Atherosclerosis*, vol. 158, no. 2, pp. 277–287, 2001.

[102] Y. Miyazaki, S. Nomura, T. Miyake, *et al.*, "High Shear Stress Can Initiate Both Platelet Aggregation and Shedding of Procoagulant Containing Microparticles," *Blood*, vol. 88, no. 9, pp. 3456–3464, Nov. 1996.

[103] J. Takagi, M. Yamada, M. Yasuda, and M. Seki, "Continuous particle separation in a microchannel having asymmetrically arranged multiple branches," *Lab on a Chip*, vol. 5, no. 7, pp. 778–784, Jun. 2005.

[104] M. Yamada, M. Nakashima, and M. Seki, "Pinched flow fractionation: Continuous size separation of particles utilizing a laminar flow profile in a pinched microchannel," *Analytical Chemistry*, vol. 76, no. 18, pp. 5465–5471, Sep. 2004.

[105] M. Yamada and M. Seki, "Hydrodynamic filtration for on-chip particle concentration and classification utilizing microfluidics," *Lab on a Chip*, vol. 5, no. 11, pp. 1233–1239, Oct. 2005.

[106] T. Yanai, T. Ouchi, M. Yamada, and M. Seki, "Hydrodynamic Microparticle Separation Mechanism Using Three-Dimensional Flow Profiles in Dual-Depth and Asymmetric Lattice-Shaped Microchannel Networks," *Micromachines 2019, Vol. 10, Page 425*, vol. 10, no. 6, p. 425, Jun. 2019.

[107] Y. Tang, J. Shi, S. Li, L. Wang, Y. E. Cayre, and Y. Chen, "Microfluidic device with integrated microfilter of conical-shaped holes for high efficiency and high purity capture of circulating tumor cells," *Scientific Reports 2014 4:1*, vol. 4, no. 1, pp. 1–7, Aug. 2014.

[108] T. Salafi, Y. Zhang, and Y. Zhang, "A Review on Deterministic Lateral Displacement for Particle Separation and Detection," *Nano-Micro Letters 2019 11:1*, vol. 11, no. 1, pp. 1–33, Sep. 2019.

[109] C. Y. Lee, C. L. Chang, Y. N. Wang, and L. M. Fu, "Microfluidic Mixing: A Review," *International Journal of Molecular Sciences 2011, Vol. 12, Pages 3263-3287*, vol. 12, no. 5, pp. 3263–3287, May 2011.

[110] S. Choi and J. K. Park, "Continuous hydrophoretic separation and sizing of microparticles using slanted obstacles in a microchannel," *Lab on a Chip*, vol. 7, no. 7, pp. 890–897, Jun. 2007.

[111] N. S. Lynn and D. S. Dandy, "Geometrical optimization of helical flow in grooved micromixers," *Lab on a Chip*, vol. 7, no. 5, pp. 580–587, May 2007.

[112] S. Choi, S. Song, C. Choi, and J. K. Park, "Continuous blood cell separation by hydrophoretic filtration," *Lab on a Chip*, vol. 7, no. 11, pp. 1532–1538, Oct. 2007.

[113] S. J. Tan, L. Yobas, G. Y. H. Lee, C. N. Ong, and C. T. Lim, "Microdevice for the isolation and enumeration of cancer cells from blood," *Biomedical Microdevices*, vol. 11, no. 4, pp. 883–892, Apr. 2009.

[114] C. H. Hsu, D. Di Carlo, C. Chen, D. Irimia, and M. Toner, "Microvortex for focusing, guiding and sorting of particles," *Lab on a Chip*, vol. 8, no. 12, pp. 2128–2134, Dec. 2008.

[115] C. I. Civin, T. Ward, A. M. Skelley, *et al.*, "Automated leukocyte processing by microfluidic deterministic lateral displacement," *Cytometry Part A*, vol. 89, no. 12, pp. 1073–1083, Dec. 2016.

[116] J. V. Green, M. Radisic, and S. K. Murthy, "Deterministic lateral displacement as a means to enrich large cells for tissue engineering," *Analytical Chemistry*, vol. 81, no. 21, pp. 9178–9182, Nov. 2009.

[117] J. T. Smith, B. H. Wunsch, N. Dogra, *et al.*, "Integrated nanoscale deterministic lateral displacement arrays for separation of extracellular vesicles from clinically-relevant volumes of biological samples," *Lab on a Chip*, vol. 18, no. 24, pp. 3913–3925, Dec. 2018.

[118] B. Zhang, J. V. Green, S. K. Murthy, and M. Radisic, "Label-Free Enrichment of Functional Cardiomyocytes Using Microfluidic Deterministic Lateral Flow Displacement," *PLOS ONE*, vol. 7, no. 5, e37619, May 2012.

[119] T. S. Tran, B. D. Ho, J. P. Beech, and J. O. Tegenfeldt, "Open channel deterministic lateral displacement for particle and cell sorting," *Lab on a Chip*, vol. 17, no. 21, pp. 3592–3600, Oct. 2017.

[120] Z. Liu, F. Huang, J. Du, *et al.*, "Rapid isolation of cancer cells using microfluidic deterministic lateral displacement structure," *Biomicrofluidics*, vol. 7, no. 1, p. 011 801, Jan. 2013.

[121] S. H. Holm, J. P. Beech, M. P. Barrett, and J. O. Tegenfeldt, "Separation of parasites from human blood using deterministic lateral displacement," *Lab on a Chip*, vol. 11, no. 7, pp. 1326–1332, Apr. 2011.

[122] M. Xavier, S. H. Holm, J. P. Beech, *et al.*, "Label-free enrichment of primary human skeletal progenitor cells using deterministic lateral displacement," *Lab on a Chip*, vol. 19, no. 3, pp. 513–523, Jan. 2019.

[123] D. W. Inglis, K. J. Morton, J. A. Davis, *et al.*, "Microfluidic device for label-free measurement of platelet activation," *Lab on a Chip*, vol. 8, no. 6, pp. 925–931, May 2008.

[124] J. McGrath, M. Jimenez, and H. Bridle, "Deterministic lateral displacement for particle separation: a review," *Lab on a Chip*, vol. 14, no. 21, pp. 4139–4158, Sep. 2014.

[125] S. L. Feng, A. M. Skelley, A. G. Anwer, G. Liu, and D. W. Inglis, "Maximizing particle concentration in deterministic lateral displacement arrays," *Biomicrofluidics*, vol. 11, no. 2, Mar. 2017.

[126] A. Aghilinejad, M. Aghaamoo, and X. Chen, "On the transport of particles/cells in high-throughput deterministic lateral displacement devices: Implications for circulating tumor cell separation," *Biomicrofluidics*, vol. 13, no. 3, p. 34 112, May 2019.

[127] D. Huang, J. Man, D. Jiang, J. Zhao, and N. Xiang, "Inertial microfluidics: Recent advances," *ELECTROPHORESIS*, vol. 41, no. 24, pp. 2166–2187, Dec. 2020.

[128] T. H. Kim, H. J. Yoon, P. Stella, and S. Nagrath, "Cascaded spiral microfluidic device for deterministic and high purity continuous separation of circulating tumor cells," *Biomicrofluidics*, vol. 8, no. 6, Dec. 2014.

[129] B. L. Khoo, M. E. Warkiani, D. S. W. Tan, *et al.*, "Clinical Validation of an Ultra High-Throughput Spiral Microfluidics for the Detection and Enrichment of Viable Circulating Tumor Cells," *PLOS ONE*, vol. 9, no. 7, e99409, Jul. 2014.

[130] N. Nivedita and I. Papautsky, "Continuous separation of blood cells in spiral microfluidic devices," *Biomicrofluidics*, vol. 7, no. 5, Sep. 2013.

[131] J. Sun, M. Li, C. Liu, *et al.*, "Double spiral microchannel for label-free tumor cell separation and enrichment," *Lab on a Chip*, vol. 12, no. 20, pp. 3952–3960, Sep. 2012.

[132] T. Y. Lee, K. A. Hyun, S. I. Kim, and H. I. Jung, "An integrated microfluidic chip for one-step isolation of circulating tumor cells," *Sensors and Actuators B: Chemical*, vol. 238, pp. 1144–1150, Jan. 2017.

[133] C. A. Aya-Bonilla, G. Marsavela, J. B. Freeman, *et al.*, "Isolation and detection of circulating tumour cells from metastatic melanoma patients using a slanted spiral microfluidic device," *Oncotarget*, vol. 8, no. 40, pp. 67 355–67 368, Jun. 2017.

[134] J. Sun, C. Liu, M. Li, *et al.*, "Size-based hydrodynamic rare tumor cell separation in curved microfluidic channels," *Biomicrofluidics*, vol. 7, no. 1, Feb. 2013.

[135] M. E. Warkiani, G. Guan, K. B. Luan, *et al.*, "Slanted spiral microfluidics for the ultra-fast, label-free isolation of circulating tumor cells," *Lab on a Chip*, vol. 14, no. 1, pp. 128–137, Nov. 2013.

[136] D. Di Carlo, "Inertial microfluidics," *Lab on a Chip*, vol. 9, no. 21, pp. 3038–3046, Nov. 2009.

[137] J. Zhou and I. Papautsky, "Fundamentals of inertial focusing in microchannels," *Lab on a Chip*, vol. 13, no. 6, pp. 1121–1132, Feb. 2013.

[138] N. Xiang and Z. Ni, "High-throughput blood cell focusing and plasma isolation using spiral inertial microfluidic devices," *Biomedical Microdevices*, vol. 17, no. 6, pp. 1–11, Dec. 2015.

[139] J. M. Martel and M. Toner, "Inertial Focusing in Microfluidics," *Annual Review of Biomedical Engineering*, vol. 16, pp. 371–396, Jul. 2014.

[140] J. Cruz, T. Graells, M. Walldén, and K. Hjort, "Inertial focusing with sub-micron resolution for separation of bacteria," *Lab on a Chip*, vol. 19, no. 7, pp. 1257–1266, Mar. 2019.

[141] X. Wang, M. Zandi, C. C. Ho, N. Kaval, and I. Papautsky, "Single stream inertial focusing in a straight microchannel," *Lab on a Chip*, vol. 15, no. 8, pp. 1812–1821, Mar. 2015.

[142] A. E. Reece, K. Kaastrup, H. D. Sikes, and J. Oakey, "Staged inertial microfluidic focusing for complex fluid enrichment," *RSC Advances*, vol. 5, no. 66, pp. 53 857–53 864, Jun. 2015.

[143] A. Volpe, C. Gaudiuso, and A. Ancona, "Sorting of Particles Using Inertial Focusing and Laminar Vortex Technology: A Review," *Micromachines 2019, Vol. 10, Page 594*, vol. 10, no. 9, p. 594, Sep. 2019.

[144] M. E. Warkiani, A. K. P. Tay, G. Guan, and J. Han, "Membrane-less microfiltration using inertial microfluidics," *Scientific Reports*, vol. 5, Jul. 2015.

[145] K. H. Han and A. B. Frazier, "Paramagnetic capture mode magnetophoretic microseparator for blood cells," *IEE Proceedings: Nanobiotechnology*, vol. 153, no. 4, pp. 67–73, 2006.

[146] K. H. Han and A. B. Frazier, "Paramagnetic capture mode magnetophoretic microseparator for high efficiency blood cell separations," *Lab on a Chip*, vol. 6, no. 2, pp. 265–273, Jan. 2006.

[147] J. D. Adams, U. Kim, and H. T. Soh, "Multitarget magnetic activated cell sorter," *Proceedings of the National Academy of Sciences*, vol. 105, no. 47, pp. 18 165–18 170, 2008. eprint: `https://www.pnas.org/doi/pdf/10.1073/pnas.0809795105`.

[148] W. Zhao, Y. Liu, B. D. Jenkins, *et al.*, "Tumor antigen-independent and cell size variation-inclusive enrichment of viable circulating tumor cells," *Lab on a Chip*, vol. 19, no. 10, pp. 1860–1876, May 2019.

[149] N. Pamme and C. Wilhelm, "Continuous sorting of magnetic cells via on-chip free-flow magnetophoresis," *Lab on a Chip*, vol. 6, no. 8, pp. 974–980, Jul. 2006.

[150] H. Cho, J. Kim, C. W. Jeon, and K. H. Han, "A disposable microfluidic device with a reusable magnetophoretic functional substrate for isolation of circulating tumor cells," *Lab on a Chip*, vol. 17, no. 23, pp. 4113–4123, Nov. 2017.

[151] B. D. Plouffe, M. Mahalanabis, L. H. Lewis, C. M. Klapperich, and S. K. Murthy, "Clinically relevant microfluidic magnetophoretic isolation of rare-cell populations for diagnostic and therapeutic monitoring applications," *Analytical Chemistry*, vol. 84, no. 3, pp. 1336–1344, Feb. 2012.

[152] J. Kim, H. Cho, S. I. Han, and K. H. Han, "Single-Cell Isolation of Circulating Tumor Cells from Whole Blood by Lateral Magnetophoretic Microseparation and Microfluidic Dispensing," *Analytical Chemistry*, vol. 88, no. 9, pp. 4857–4863, May 2016.

[153] Y. Jiang, H. Wang, S. Li, and W. Wen, "Applications of Micro/Nanoparticles in Microfluidic Sensors: A Review," *Sensors 2014, Vol. 14, Pages 6952-6964*, vol. 14, no. 4, pp. 6952–6964, Apr. 2014.

[154] B. Techaumnat, N. Panklang, A. Wisitsoraat, and Y. Suzuki, "Study on the discrete dielectrophoresis for particle–cell separation," *ELECTROPHORESIS*, vol. 41, no. 10-11, pp. 991–1001, 2020.

[155] Y. Ai, C. K. Sanders, and B. L. Marrone, "Separation of escherichia coli bacteria from peripheral blood mononuclear cells using standing surface acoustic waves," *Analytical Chemistry*, vol. 85, no. 19, pp. 9126–9134, Oct. 2013.

[156] P. R. C. Gascoyne and S. Shim, "Isolation of circulating tumor cells by dielectrophoresis," *Cancers*, vol. 6, no. 1, pp. 545–579, 2014.

[157] U. Kim, C. W. Shu, K. Y. Dane, P. S. Daugherty, J. Y. Wang, and H. T. Soh, "Selection of mammalian cells based on their cell-cycle phase using dielectrophoresis," *Proceedings of the National Academy of Sciences of the United States of America*, vol. 104, no. 52, pp. 20 708–20 712, Dec. 2007.

[158] T. N. Adams, A. Y. Jiang, P. D. Vyas, and L. A. Flanagan, "Separation of neural stem cells by whole cell membrane capacitance using dielectrophoresis," *Methods*, vol. 133, pp. 91–103, Jan. 2018.

[159] J. An, J. Lee, S. H. Lee, J. Park, and B. Kim, "Separation of malignant human breast cancer epithelial cells from healthy epithelial cells using an advanced dielectrophoresis-activated cell sorter (DACS)," *Analytical and Bioanalytical Chemistry*, vol. 394, no. 3, pp. 801–809, Jun. 2009.

[160] B. Çetin and D. Li, "Lab-on-a-chip device for continuous particle and cell separation based on electrical properties via alternating current dielectrophoresis," *ELECTROPHORESIS*, vol. 31, no. 18, pp. 3035–3043, Sep. 2010.

[161] S. H. Ling, Y. C. Lam, and K. S. Chian, "Continuous cell separation using dielectrophoresis through asymmetric and periodic microelectrode array," *Analytical Chemistry*, vol. 84, no. 15, pp. 6463–6470, Aug. 2012.

[162] J. Yoshioka, Y. Ohsugi, T. Yoshitomi, T. Yasukawa, N. Sasaki, and K. Yoshimoto, "Label-Free Rapid Separation and Enrichment of Bone Marrow-Derived Mesenchymal Stem Cells from a Heterogeneous Cell Mixture Using a Dielectrophoresis Device," *Sensors 2018, Vol. 18, Page 3007*, vol. 18, no. 9, p. 3007, Sep. 2018.

[163] A. Shamloo and A. Kamali, "Numerical analysis of a dielectrophoresis field-flow fractionation device for the separation of multiple cell types," *Journal of Separation Science*, vol. 40, no. 20, pp. 4067–4075, Oct. 2017.

[164] K. Zhao, Larasati, B. P. Duncker, and D. Li, "Continuous Cell Characterization and Separation by Microfluidic Alternating Current Dielectrophoresis," *Analytical Chemistry*, vol. 91, no. 9, pp. 6304–6314, May 2019.

[165] M. A. Burguillos, C. Magnusson, M. Nordin, *et al.*, "Microchannel Acoustophoresis does not Impact Survival or Function of Microglia, Leukocytes or Tumor Cells," *PLOS ONE*, vol. 8, no. 5, e64233, May 2013.

[166] J. Hultström, O. Manneberg, K. Dopf, H. Hertz, H. Brismar, and M. Wiklund, "Proliferation and viability of adherent cells manipulated by standing-wave ultrasound in a microfluidic chip," *Ultrasound in Medicine & Biology*, vol. 33, no. 1, pp. 145–151, 2007.

[167] M. Wiklund, "Acoustofluidics 12: Biocompatibility and cell viability in microfluidic acoustic resonators," *Lab on a Chip*, vol. 12, no. 11, pp. 2018–2028, May 2012.

[168] J. J. Hawkes, R. W. Barber, D. R. Emerson, and W. T. Coakley, "Continuous cell washing and mixing driven by an ultrasound standing wave within a microfluidic channel," *Lab on a Chip*, vol. 4, no. 5, pp. 446–452, Oct. 2004.

[169] J. D. Adams, C. L. Ebbesen, R. Barnkob, A. H. Yang, H. T. Soh, and H. Bruus, "High-throughput, temperature-controlled microchannel acoustophoresis device made with rapid prototyping," *Journal of Micromechanics and Microengineering*, vol. 22, no. 7, p. 075 017, Jun. 2012.

[170] W. Qiu, T. Baasch, and T. Laurell, "Enhancement of Acoustic Energy Density in Bulk-Wave-Acoustophoresis Devices Using Side Actuation," *Physical Review Applied*, vol. 17, no. 4, p. 044 043, Apr. 2022.

[171] J. Gui, H. Jiang, Y. Chen, *et al.*, "High-throughput acoustic separation device with impedance-matched channel," *Microfluidics and Nanofluidics*, vol. 27, no. 9, pp. 1–6, Sep. 2023.

[172] M. Gedge and M. Hill, "Acoustofluidics 17: Theory and applications of surface acoustic wave devices for particle manipulation," *Lab on a Chip*, vol. 12, no. 17, pp. 2998–3007, Jul. 2012.

[173] M. Wu, A. Ozcelik, J. Rufo, Z. Wang, R. Fang, and T. Jun Huang, "Acoustofluidic separation of cells and particles," *Microsystems & Nanoengineering 2019 5:1*, vol. 5, no. 1, pp. 1–18, Jun. 2019.

[174] S. C. S. Lin, X. Mao, and T. J. Huang, "Surface acoustic wave (SAW) acoustophoresis: now and beyond," *Lab on a Chip*, vol. 12, no. 16, pp. 2766–2770, Jul. 2012.

[175] S. Li, X. Ding, Z. Mao, *et al.*, "Standing surface acoustic wave (SSAW)-based cell washing," *Lab on a Chip*, vol. 15, no. 1, pp. 331–338, Dec. 2014.

[176] H. Li, J. R. Friend, and L. Y. Yeo, "Surface acoustic wave concentration of particle and bioparticle suspensions," *Biomedical Microdevices*, vol. 9, no. 5, pp. 647–656, Oct. 2007.

[177] M. Dao, S. Suresh, T. J. Huang, *et al.*, "Acoustic separation of circulating tumor cells," *Proceedings of the National Academy of Sciences of the United States of America*, vol. 112, no. 16, pp. 4970–4975, Apr. 2015.

[178] S. Sepehrirahnama, A. Ray Mohapatra, S. Oberst, Y. K. Chiang, D. A. Powell, and K. M. Lim, "Acoustofluidics 24: theory and experimental measurements of acoustic interaction force," *Lab on a Chip*, vol. 22, no. 18, pp. 3290–3313, Sep. 2022.

[179] J. Rufo, F. Cai, J. Friend, M. Wiklund, and T. J. Huang, "Acoustofluidics for biomedical applications," *Nature Reviews Methods Primers 2022 2:1*, vol. 2, no. 1, pp. 1–21, Apr. 2022.

[180] Y. Fan, X. Wang, J. Ren, F. Lin, and J. Wu, "Recent advances in acoustofluidic separation technology in biology," *Microsystems & Nanoengineering 2022 8:1*, vol. 8, no. 1, pp. 1–16, Sep. 2022.

[181] J. Heyman, *Acoustophoresis method and apparatus*. US Patent 5,147,562, Sept. 15 1992.

[182] *Acoustophoresis separation method*. US Patent 5,192,450, Mar.9 1993.

[183] P. Augustsson, *On microchannel acoustophoresis - Experimental considerations and life science applications*. Ph.D. thesis, Lund University, 2011.

[184] R. Barnkob, *Physics of microparticle acoustophoresis - Bridging theory and experiment*. Ph.D. thesis, Technical University of Denmark - DTU, 2012.

[185] J. Karlsen, *Theory of nonlinear acoustic forces acting on fluids and particles in microsystems*. Ph.D. thesis, Technical University of Denmark - DTU, 2018.

[186] A. Lenshof, M. Evander, T. Laurell, and J. Nilsson, "Acoustofluidics 5: Building microfluidic acoustic resonators," *Lab on a Chip*, vol. 12, no. 4, pp. 684–695, Jan. 2012.

[187] H. Bruus, "Acoustofluidics 2: Perturbation theory and ultrasound resonance modes," *Lab on a Chip*, vol. 12, no. 1, pp. 20–28, Dec. 2011.

[188] L. E. Kinsler, A. R. Frey, A. B. Coppens, and J. V. Sanders, *Fundamentals of Acoustics*. 4th ed., (John Wiley & Sons), 2000.

[189] L. P. Gor'kov, "On the forces acting on a small particle in an acoustical field in an ideal fluid," *Selected Papers of Lev P. Gor'kov*, pp. 315–317, Jan. 2014.

[190] L. V. King, "On the acoustic radiation pressure on spheres," *Proceedings of The Royal Society A: Mathematical, Physical and Engineering Sciences*, vol. 147, pp. 212–240, 1934.

[191] K. Yosioka, "Acoustic radiation pressure on a compressible sphere," *Acustica*, vol. 5, pp. 167–173, 1955.

[192] M. Settnes and H. Bruus, "Forces acting on a small particle in an acoustical field in a viscous fluid," *Physical Review E - Statistical, Nonlinear, and Soft Matter Physics*, vol. 85, no. 1, p. 016 327, Jan. 2012.

[193] L. M. Andersen, A. Nysteen, and M. Settnes, *Forces acting on microparticles in acoustofluidic systems*. Master's thesis, DTU Nanotech, Technical University of Denmark, 2009.

[194] H. Bruus, "Acoustofluidics 7: The acoustic radiation force on small particles," *Lab on a Chip*, vol. 12, no. 6, pp. 1014–1021, Feb. 2012.

[195] H. Bruus, "Acoustofluidics 10: Scaling laws in acoustophoresis," *Lab on a Chip*, vol. 12, no. 9, pp. 1578–1586, Apr. 2012.

[196] C. Grenvall, P. Augustsson, J. R. Folkenberg, and T. Laurell, "Harmonic microchip acoustophoresis: A route to online raw milk sample precondition in protein and lipid content quality control," *Analytical Chemistry*, vol. 81, no. 15, pp. 6195–6200, Aug. 2009.

[197] L. Rayleigh, "I. On the circulation of air observed in Kundt's tubes, and on some allied acoustical problems," *Philosophical Transactions of the Royal Society of London*, vol. 175, pp. 1–21, Dec. 1884.

[198] M. Rezayati Charan, F. Berg, and P. Augustsson, "Acoustofluidic Three-Dimensional Motion of Suspended Cells at Near-Zero Acoustic Contrast in Homogeneous Media," *Physical Review Applied*, vol. 19, no. 1, p. 014 046, Jan. 2023.

[199] M. Rezayati Charan and P. Augustsson, "Acoustophoretic characterization and separation of blood cells in acoustic impedance gradients," *Phys. Rev. Appl.*, vol. 20, p. 024 066, 2 2023.

[200] R. Barnkob, P. Augustsson, T. Laurell, and H. Bruus, "Acoustic radiation- and streaming-induced microparticle velocities determined by microparticle image velocimetry in an ultrasound symmetry plane," *Physical Review E - Statistical, Nonlinear, and Soft Matter Physics*, vol. 86, no. 5, p. 056 307, Nov. 2012.

[201] M. W. Ley and H. Bruus, "Continuum modeling of hydrodynamic particle–particle interactions in microfluidic high-concentration suspensions," *Lab on a Chip*, vol. 16, no. 7, pp. 1178–1188, Mar. 2016.

[202] Z. Mandralis, "Transient response of fine particle suspensions to mild planar ultrasonic fields," Ph.D. dissertation, Case Western Reserve University, 1990.

[203] M. W. H. Ley, *Effective modelling of acoustofluidic devices*. PhD thesis, Department of Physics, Technical University of Denmark, 2017.

[204] P. B. Muller, R. Barnkob, M. J. H. Jensen, and H. Bruus, "A numerical study of microparticle acoustophoresis driven by acoustic radiation forces and streaming-induced drag forces," *Lab on a Chip*, vol. 12, no. 22, pp. 4617–4627, Oct. 2012.

[205] M. Antfolk and T. Laurell, "Continuous flow microfluidic separation and processing of rare cells and bioparticles found in blood – A review," *Analytica Chimica Acta*, vol. 965, pp. 9–35, May 2017.

[206] O. Jakobsson, S. S. Oh, M. Antfolk, M. Eisenstein, T. Laurell, and H. T. Soh, "Thousand-Fold Volumetric Concentration of Live Cells with a Recirculating Acoustofluidic Device," *Analytical Chemistry*, vol. 87, no. 16, pp. 8497–8502, Aug. 2015.

[207] M. Nordin and T. Laurell, "Two-hundredfold volume concentration of dilute cell and particle suspensions using chip integrated multistage acousto-phoresis," *Lab on a Chip*, vol. 12, no. 22, pp. 4610–4616, Oct. 2012.

[208] D. Carugo, T. Octon, W. Messaoudi, *et al.*, "A thin-reflector microfluidic resonator for continuous-flow concentration of microorganisms: a new approach to water quality analysis using acoustofluidics," *Lab on a Chip*, vol. 14, no. 19, pp. 3830–3842, Aug. 2014.

[209] A. Lenshof, A. Ahmad-Tajudin, K. Järås, *et al.*, "Acoustic whole blood plasmapheresis chip for prostate specific antigen microarray diagnostics," *Analytical Chemistry*, vol. 81, no. 15, pp. 6030–6037, Aug. 2009.

[210] P. Augustsson and T. Laurell, "Acoustofluidics 11: Affinity specific extraction and sample decomplexing using continuous flow acoustophoresis," *Lab on a Chip*, vol. 12, no. 10, pp. 1742–1752, Apr. 2012.

[211] F. Petersson, L. Åberg, A. M. Swärd-Nilsson, and T. Laurell, "Free flow acoustophoresis: Microfluidic-based mode of particle and cell separation," *Analytical Chemistry*, vol. 79, no. 14, pp. 5117–5123, Jul. 2007.

[212] P. Thévoz, J. D. Adams, H. Shea, H. Bruus, and H. T. Soh, "Acoustophoretic synchronization of mammalian cells in microchannels," *Analytical Chemistry*, vol. 82, no. 7, pp. 3094–3098, Apr. 2010.

[213] M. Ann, H Weiser, R. E. Apfel, and H Weiser ', "Extension of acoustic levitation to include the study of micron-size particles in a more compressible host liquid," *The Journal of the Acoustical Society of America*, vol. 71, no. 5, pp. 1261–1268, May 1982.

[214] J. Dykes, A. Lenshof, I. B. Åstrand-Grundström, T. Laurell, and S. Scheding, "Efficient Removal of Platelets from Peripheral Blood Progenitor Cell Products Using a Novel Micro-Chip Based Acoustophoretic Platform," *PLOS ONE*, vol. 6, no. 8, e23074, 2011.

[215] C. W. Shields, L. M. Johnson, L. Gao, and G. P. López, "Elastomeric negative acoustic contrast particles for capture, acoustophoretic transport, and confinement of cells in microfluidic systems," *Langmuir*, vol. 30, no. 14, pp. 3923–3927, Apr. 2014.

[216] P. Ohlsson, K. Petersson, P. Augustsson, and T. Laurell, "Acoustic impe-dance matched buffers enable separation of bacteria from blood cells at high cell concentrations," *Scientific Reports 2018 8:1*, vol. 8, no. 1, pp. 1–11, Jun. 2018.

[217] D. Van Assche, E. Reithuber, W. Qiu, *et al.*, "Gradient acoustic focusing of sub-micron particles for separation of bacteria from blood lysate," *Scientific Reports 2020 10:1*, vol. 10, no. 1, pp. 1–13, Feb. 2020.

[218] J. F. Greenleaf, M. Fatemi, and M. Insana, "Selected Methods for Imaging Elastic Properties of Biological Tissues," *Annu Rev Biomed Eng*, vol. 5, pp. 57–78, Nov. 2003.

[219] K. Nightingale, "Acoustic Radiation Force Impulse (ARFI) Imaging: A Review," *Current Medical Imaging Reviews*, vol. 7, no. 4, pp. 328–339, Nov. 2011.

[220] J. A. Hildebrand, D. Rugar, R. N. Johnston, and C. F. Quate, "Acoustic microscopy of living cells," *Proceedings of the National Academy of Sciences*, vol. 78, no. 3, pp. 1656–1660, Mar. 1981.

[221] T. Kundu, J. Bereiter-Hahn, and I. Karl, "Cell Property Determination from the Acoustic Microscope Generated Voltage Versus Frequency Curves," *Biophysical Journal*, vol. 78, no. 5, pp. 2270–2279, May 2000.

[222] E. M. Strohm, G. J. Czarnota, and M. C. Kolios, "Quantitative measurements of apoptotic cell properties using acoustic microscopy," *IEEE Transactions on Ultrasonics, Ferroelectrics, and Frequency Control*, vol. – 57, no. 10, pp. 2293–2304, Oct. 2010.

[223] E. C. Weiss, P. Anastasiadis, G. Pilarczyk, R. M. Lemor, and P. V. Zinin, "Mechanical properties of single cells by high-frequency time-resolved acoustic microscopy," *IEEE Transactions on Ultrasonics, Ferroelectrics, and Frequency Control*, vol. 54, no. 11, pp. 2257–2271, Nov. 2007.

[224] K. W. Cushing, F. Garofalo, C. Magnusson, L. Ekblad, H. Bruus, and T. Laurell, "Ultrasound Characterization of Microbead and Cell Suspensions by Speed of Sound Measurements of Neutrally Buoyant Samples," *Analytical Chemistry*, vol. 89, no. 17, pp. 8917–8923, Sep. 2017.

[225] P. Augustsson, J. T. Karlsen, H. W. Su, H. Bruus, and J. Voldman, "Iso-acoustic focusing of cells for size-insensitive acousto-mechanical phenotyping," *Nature Communications 2016 7:1*, vol. 7, no. 1, pp. 1–9, May 2016.

[226] D. Hartono, Y. Liu, P. L. Tan, X. Y. S. Then, L. Y. L. Yung, and K. M. Lim, "On-chip measurements of cell compressibility via acoustic radiation," *Lab on a Chip*, vol. 11, no. 23, pp. 4072–4080, Nov. 2011.

[227] Q. Fu, Y. Zhang, T. Huang, Y. Liang, and Y. Liu, "Measurement of cell compressibility changes during epithelial-mesenchymal transition based on acoustofluidic microdevice," *Biomicrofluidics*, vol. 15, no. 6, p. 64 101, Dec. 2021.

[228] H. Wang, Z. Liu, D. M. Shin, *et al.*, "A continuous-flow acoustofluidic cytometer for single-cell mechanotyping," *Lab on a Chip*, vol. 19, no. 3, pp. 387–393, Jan. 2019.

[229] T. Yang, F. Bragheri, G. Nava, *et al.*, "A comprehensive strategy for the analysis of acoustic compressibility and optical deformability on single cells," *Scientific Reports 2016 6:1*, vol. 6, no. 1, pp. 1–13, Apr. 2016.

[230] Y. Wu, A. G. Stewart, and P. V. Lee, "On-chip cell mechanophenotyping using phase modulated surface acoustic wave," *Biomicrofluidics*, vol. 13, no. 2, p. 24 107, Mar. 2019.

[231] Y. Wu, A. G. Stewart, and P. V. Lee, "High-throughput microfluidic compressibility cytometry using multi-tilted-angle surface acoustic wave," *Lab on a Chip*, vol. 21, no. 14, pp. 2812–2824, Jul. 2021.

[232] H. Wang, Z. Liu, D. M. Shin, *et al.*, "Single-cell compressibility quantification for assessing metastatic potential of cancer cells through multi-frequency acoustophoresis," *Microfluidics and Nanofluidics*, vol. 22, no. 6, pp. 1–7, Jun. 2018.

[233] A. Edthofer, J. Novotny, A. Lenshof, T. Laurell, and T. Baasch, "Acoustofluidic Properties of Polystyrene Microparticles," *Analytical Chemistry*, vol. 95, pp. 10 346–10 352, Jul. 2023.

[234] J. T. Karlsen, W. Qiu, P. Augustsson, and H. Bruus, "Acoustic streaming and its suppression in inhomogeneous fluids," *Phys. Rev. Lett.*, vol. -120, p. 054 501, 5 Jan. 2018.

[235] W. Qiu, J. T. Karlsen, H. Bruus, and P. Augustsson, "Experimental Characterization of Acoustic Streaming in Gradients of Density and Compressibility," *Physical Review Applied*, vol. 11, no. 2, p. 024 018, Feb. 2019.

[236] S. Karthick, P. N. Pradeep, P. Kanchana, and A. K. Sen, "Acoustic impedance-based size-independent isolation of circulating tumour cells from blood using acoustophoresis," *Lab on a Chip*, vol. 18, no. 24, pp. 3802–3813, Dec. 2018.

[237] S. Deshmukh, Z. Brzozka, T. Laurell, and P. Augustsson, "Acoustic radiation forces at liquid interfaces impact the performance of acoustophoresis," *Lab on a Chip*, vol. 14, no. 17, pp. 3394–3400, Jul. 2014.

[238] J. T. Karlsen, P. Augustsson, and H. Bruus, "Acoustic Force Density Acting on Inhomogeneous Fluids in Acoustic Fields," *Physical Review Letters*, vol. 117, no. 11, p. 114 504, Sep. 2016.

[239] J. T. Karlsen and H. Bruus, "Acoustic Tweezing and Patterning of Concentration Fields in Microfluidics," *Physical Review Applied*, vol. 7, no. 3, p. 034 017, Mar. 2017.

[240] W. Qiu, H. Bruus, and P. Augustsson, "Particle-size-dependent acoustophoretic motion and depletion of micro- And nano-particles at long timescales," *Physical Review E*, vol. 102, no. 1, p. 013 108, Jul. 2020.

[241] P. Augustsson, C. Magnusson, M. Nordin, H. Lilja, and T. Laurell, "Microfluidic, label-free enrichment of prostate cancer cells in blood based on acoustophoresis," *Analytical Chemistry*, vol. 84, no. 18, pp. 7954–7962, Sep. 2012.

[242] O. Jakobsson, C. Grenvall, M. Nordin, M. Evander, and T. Laurell, "Acoustic actuated fluorescence activated sorting of microparticles," *Lab on a Chip*, vol. 14, no. 11, pp. 1943–1950, May 2014.

[243] C. Grenvall, C. Antfolk, C. Z. Bisgaard, and T. Laurell, "Two-dimensional acoustic particle focusing enables sheathless chip Coulter counter with planar electrode configuration," *Lab on a Chip*, vol. 14, no. 24, pp. 4629–4637, Nov. 2014.

[244] M. Baudoin, J. L. Thomas, R. A. Sahely, *et al.*, "Spatially selective manipulation of cells with single-beam acoustical tweezers," *Nature Communications 2020 11:1*, vol. 11, no. 1, pp. 1–10, Aug. 2020.

[245] P. Sehgal and B. J. Kirby, "Separation of 300 and 100 nm Particles in Fabry-Perot Acoustofluidic Resonators," *Analytical Chemistry*, vol. 89, no. 22, pp. 12 192–12 200, Nov. 2017.

[246] M. Bora and M. Shusteff, "Efficient coupling of acoustic modes in microfluidic channel devices," *Lab on a Chip*, vol. 15, no. 15, pp. 3192–3202, Jul. 2015.

[247] A. Tahmasebipour, L. Friedrich, M. Begley, H. Bruus, C. Meinhart, and A. Phys Lett, "Toward optimal acoustophoretic microparticle manipulation by exploiting asymmetry," *The Journal of the Acoustical Society of America*, vol. 148, no. 1, pp. 359–373, Jul. 2020.

[248] I. Leibacher, P. Reichert, and J. Dual, "Microfluidic droplet handling by bulk acoustic wave (BAW) acoustophoresis," *Lab on a Chip*, vol. 15, no. 13, pp. 2896–2905, Jun. 2015.

[249] A. Fornell, J. Nilsson, L. Jonsson, P. K. Periyannan Rajeswari, H. N. Joensson, and M. Tenje, "Controlled Lateral Positioning of Microparticles Inside Droplets Using Acoustophoresis," *Analytical Chemistry*, vol. 87, no. 20, pp. 10 521–10 526, Oct. 2015.

[250] P. Augustsson, R. Barnkob, S. T. Wereley, H. Bruus, and T. Laurell, "Automated and temperature-controlled micro-PIV measurements enabling long-term-stable microchannel acoustophoresis characterization," *Lab on a Chip*, vol. 11, no. 24, pp. 4152–4164, Nov. 2011.